International Atomic Energy Agency

INDC(CCP)-293/L

INDC INTERNATIONAL NUCLEAR DATA COMMITTEE

TRANSLATION OF SELECTED PAPERS PUBLISHED IN NUCLEAR CONSTANTS 3, 1985

(Original Report in Russian was distributed as INDC(CCP)-252/G)

Translated by the IAEA

January 1989

IAEA NUCLEAR DATA SECTION, WAGRAMERSTRASSE 5, A-1400 VIENNA

TRANSLATION OF SELECTED PAPERS PUBLISHED

IN NUCLEAR CONSTANTS 3, 1985

(Original Report in Russian was distributed
as INDC(CCP)-252/G)

Translated by the IAEA

January 1989

Reproduced by the IAEA in Austria
January 1989

89-00154

Contents

ABSOLUTE MEASUREMENTS OF THE PROMPT NEUTRON SPECTRUM PRODUCED BY SPONTANEOUS FISSION OF ^{252}Cf IN THE LOW-ENERGY REGION

P.P. Dyachenko, E.A. Seregina, L.C. Kutsaeva,
A. Lajtai

Experimental research into the integral spectrum of neutrons produced by the spontaneous fission of ^{252}Cf has lately met with considerable success. New precision measurements of the spectrum over a wide energy range from 1 keV to 30 MeV have yielded results which are largely in good agreement with each other [1-8]. A consultative meeting of IAEA specialists [9] pointed out the need for a fresh evaluation of the integral fission neutron spectrum of ^{252}Cf in the light of recent experimental data - an evaluation which could be used as an international standard. To this end, researchers were asked to present the results of their measurements in tabular form, together with numerical data on the errors and the corrections introduced.

The results of our measurements of the fission neutron spectrum of ^{252}Cf in the range $0.02 < E < 1.22$ MeV were reported earlier [6, 7]. In the present paper we follow the recommendations of Ref. [9] and provide a more detailed description of the measurement method and the procedures used in processing the results, giving refined data on systematic errors as well as numerical data on neutron-energy dependent statistical and systematic errors.

Measurement method

Figure 1 is a diagram of the experiment. The fission fragment detector used was a fast ionization fission chamber filled with a gas mixture (90% argon, 10% carbon dioxide) at 3×10^5 Pa. The body of the chamber was a stainless steel cylinder 38 mm in diameter and 120 mm high, with walls approximately 0.1 mm thick. The electrodes, also in stainless steel, were set 1.5 mm apart and measured 25 mm in diameter and 0.1 mm in thickness. In the centre of one of these was an opening 10 mm in diameter, on which was fixed a section of platinum foil 0.05 mm thick. A thin film of californium 7 mm in diameter was applied to the foil. This layer, with a fission rate of

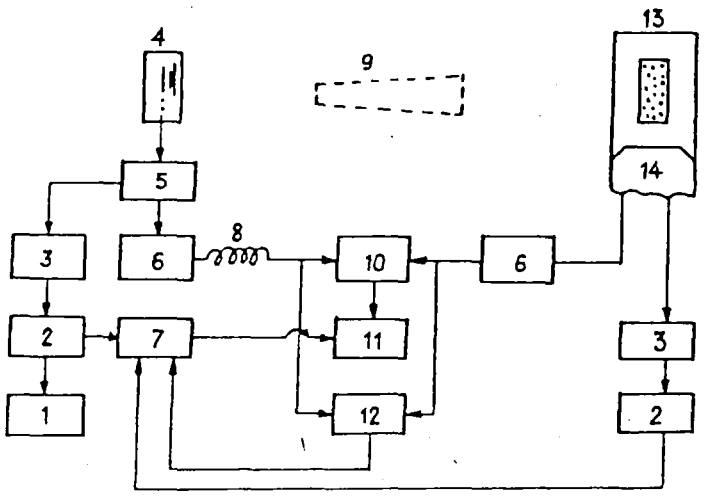

Fig. 1: Schematic diagram of the experiment.

1 - Fission fragment scaler.
2 - Integral discriminator.
3 - Slow amplifier.
4 - Fission chamber with ^{252}Cf layer.
5 - Fast amplifier.
6 - Servo threshold discriminator.
7 - Coincidence circuit.
8 - 270 ns delay line.
9 - Shadow cone.
10 - Time-amplitude converter.
11 - Analyser.
12 - Double pulse discriminator.
13 - NE-912 or NE-913 neutron detector.
14 - FEU-30 photomultiplier.

10^4 s^{-1}, was obtained by electrolysis from material which had first been carefully cleansed of both inert and radioactive impurities. The voltage applied across the electrodes was 500 V. The pulse height spectrum from the fission fragments (Fig. 2a) shows that the fission fragment and α-particle pulses are widely separated, and divided by the slow-channel threshold. This confirms the high quality of the ^{252}Cf film used in the experiment. The unusual shape of the fission fragment spectrum towards the higher energies is due to the fact that an amplifier-clipper was used to amplify the signals in the fast fission fragment channel. The fission fragment detection efficiency of the ionization chamber was 99%.

The neutron detector used was an NE-912 lithium glass (thickness 9.5 mm; diameter 45 mm), in conjunction with an FEU-30 photomultiplier. To measure the delayed α background, the NE-912 lithium glass was replaced by an NE-913 lithium glass of the same dimensions which was not sensitive to neutrons in the energy range of intent [10]. The glass was suspended in the centre of a thin-walled aluminium chamber with an inlet window 0.08 mm thick, mounted on the photocathode of the photomultiplier. The design and specification of the neutron detector are described in greater detail in Refs [11] and [12].

It must be emphasized that both the fission fragment detector and especially the neutron detector used in the experiment were designed to keep

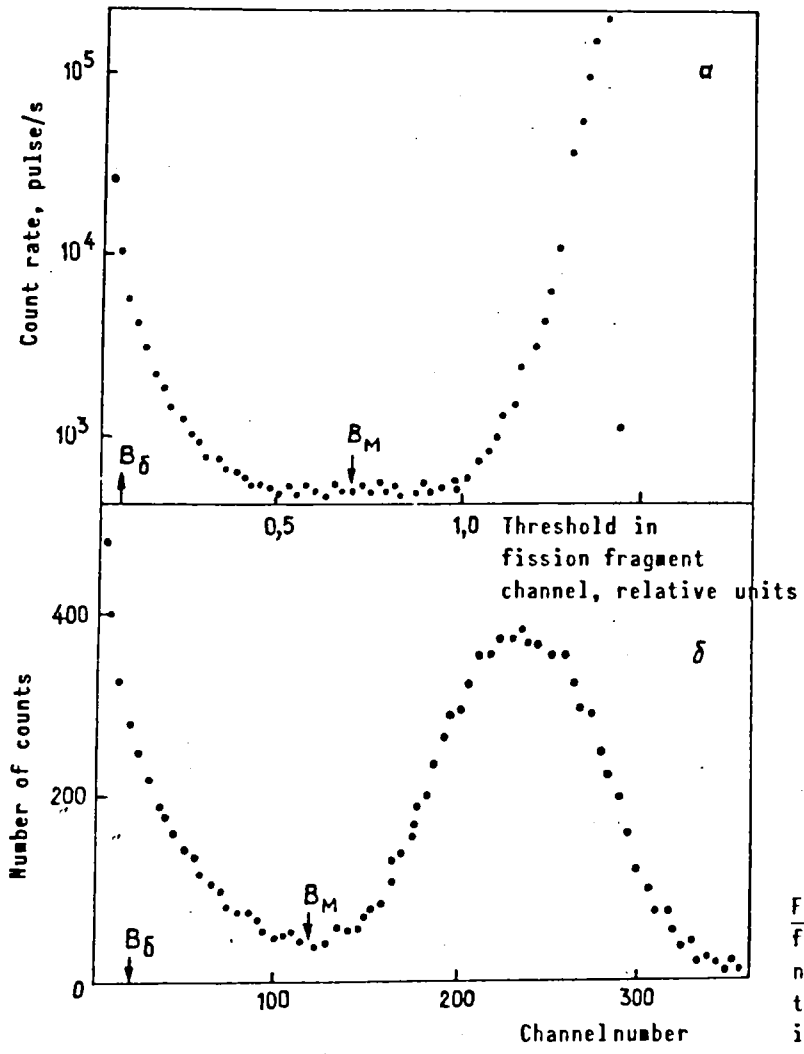

Fig. 2: Pulse height spectrum of fission fragments (a) and thermal neutrons (δ). B_δ is the detection threshold in the fast channel, B_M in the slow channel.

the amount of scattering material present in the vicinity of the solid angle of neutron detection of Ω (the angle through which the lithium glass is seen from the neutron source) to a minimum. Allowance was made, in calculating the response function of the spectrometer, for distortion of the spectrum caused by scattering of neutrons in these materials (air, the support used for californium film, the walls of the chamber and the detector inlet window), as well as for uncertainty in path lengths and scattering in the time of flight due to neutron straying in the glass. The effect of structural materials outside the solid angle of neutron detection was taken into account by the shadow cone method in measuring the scattered neutron background (a shadow cone of copper 12 cm in length was used).

In order to screen out chance pulse pile-ups, a special electronic

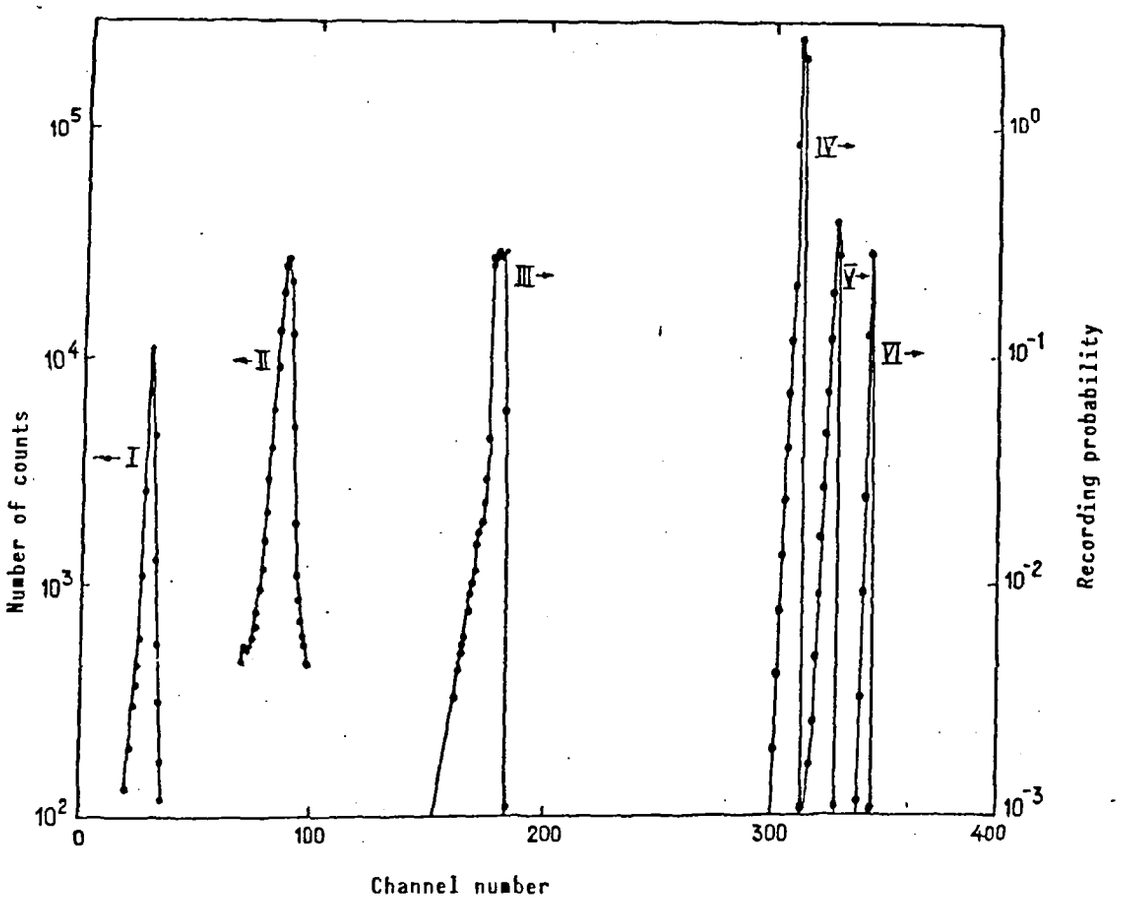

Fig. 3: Response function: I and II are measured $F_f(t,t')$, $F_n(t,t')$; III-VI are calculated $F''(E,t)$ for neutron energies of 0.025, 0.245, 0.445 and 1.220 MeV, respectively.

circuit (double-signal discriminator) was incorporated in the slow channel of the spectrometer [13]. This permitted greater accuracy of measurement.

The basic specifications of the spectrometer were as follows: time-of-flight path length $L = (30 \pm 0.1)$ cm, analyser channel width $\tau = (0.704 \pm 0.02)$ ns, solid angle of neutron detection $\Omega = (0.0176 \pm 0.0002)$ sr. Figures 2 and 3 show pulse height spectra for neutrons and fission fragments, the positions of discrimination thresholds in the fast and slow channels, and the instrument response functions for the fast channels. The last of these were measured with a stilbene detector having an intrinsic time resolution of 0.5 ns. The fission fragment channel was studied from fission gamma rays, and the neutron channel from γ-γ coincidences of ^{60}Co. The integral and differential non-linearity of the spectrometer did not exceed 0.5% and 0.7%, respectively.

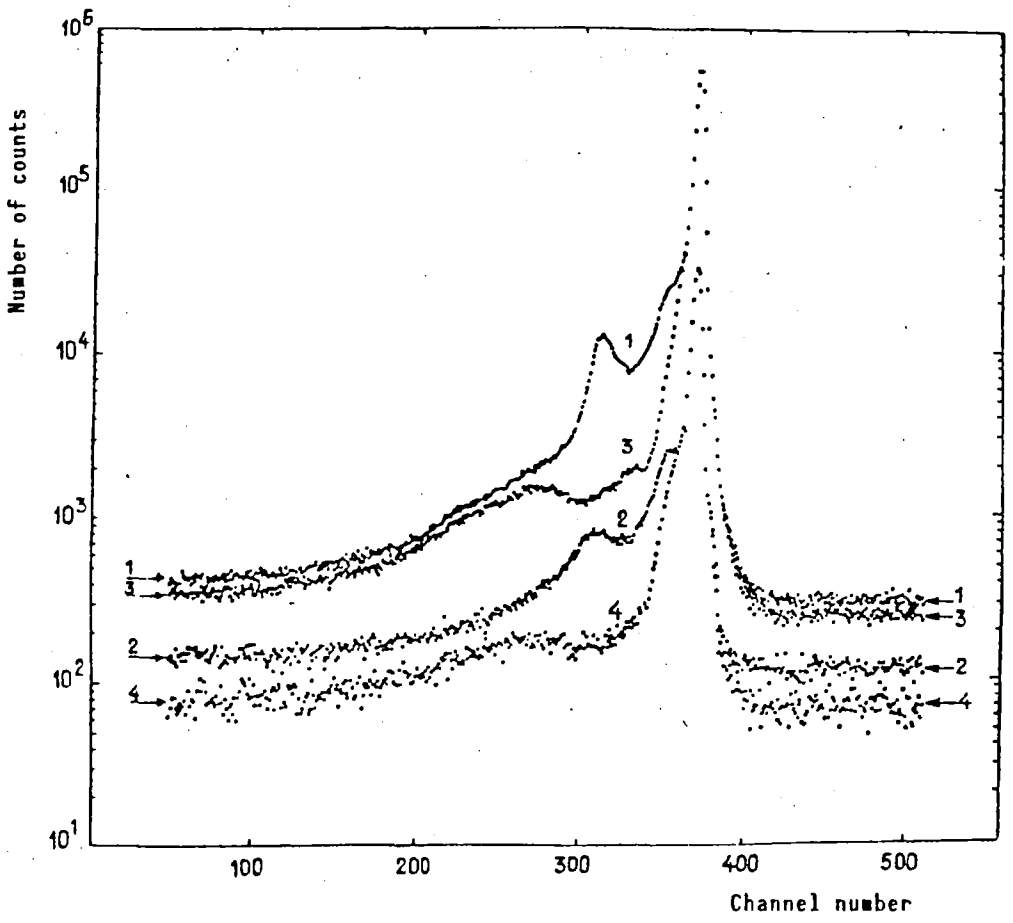

Fig. 4: Total instrument distribution obtained experimentally:
1 - NE-912; 2 - NE-912 (with cone); 3 - NE-913;
4 - NE-913 (with cone).

A cyclical system of measurements was established with four separate measurements per cycle: NE-912 readings, NE-912 with cone, NE-913, and NE-913 with cone. Each of these measurements was performed over a 24 hour period, and the experiment as a whole lasted three months without interruption. During this time 20 full cycles were carried out and $(1.523 \pm 0.015) \times 10^{10}$ fission events were recorded for each type of measurement. Figure 4 shows the resulting distributions of $P_i(t)$, which constitute measured time distributions for each of the above-mentioned types of measurement. For this purpose the number of the channel corresponding to zero time (allowing for the time-of-flight of the gamma rays) was 374 ± 0.5. A number of instrument distributions, comprising approximately channels 420 to 510, were used to determine the random coincidence background for each type of measurement.

Treatment of the results

In the general case, to extract neutron spectrum results from a measured time distribution we must solve the Fredholm integral equation of the first kind:

$$P(t) = \int F(E,t)\varphi(E)dE \qquad (1)$$

where P(t) is the measured spectrum, F(E,t) is the spectrometer response function and $\phi(E)$ is the prompt fission neutron spectrum.

It is not difficult to show that the traditional method of constructing energy spectra from measured time distributions by conversion of co-ordinates is nothing other than a solution of Eq. (1) for the particular case where the response function of the spectrometer can be defined in the form $F(E,t) = \delta[t-t(E)]\varepsilon(E)$, where $\delta[t-t(E)]$ is a delta-function, and $\varepsilon(E)$ is the neutron detection efficiency. This representation of the spectrometer response function is an idealization of the problem, however, and in some cases - particularly when small path lengths are used - can lead to substantial error.

It is unfortunately not possible at present to obtain sufficiently precise measurements or calculations of the function F(E,t) in absolute units, and there are, furthermore, certain difficulties in solving Eq. (1). For this reason, an indirect method was used to determine the difference between a realistic spectrometer response function and the δ-function, and results were processed in the manner described below.

Firstly, the random coincident background was subtracted from all the measured distributions of $P_i(t)$. Next, the background of neutrons and gamma rays scattered by structural materials outside the solid angle of detection and the background of delayed fission gamma rays were calculated according to the expression $P(t) = P_1(t) - P_2(t) - P_3(t) + P_4(t)$. The $P_2(t)$ spectrum was first corrected to allow for the transmission of the shadow cone. In the range up to 500 keV this correction was less than 0.5%; it rose to between 2 and 4% at higher energies.

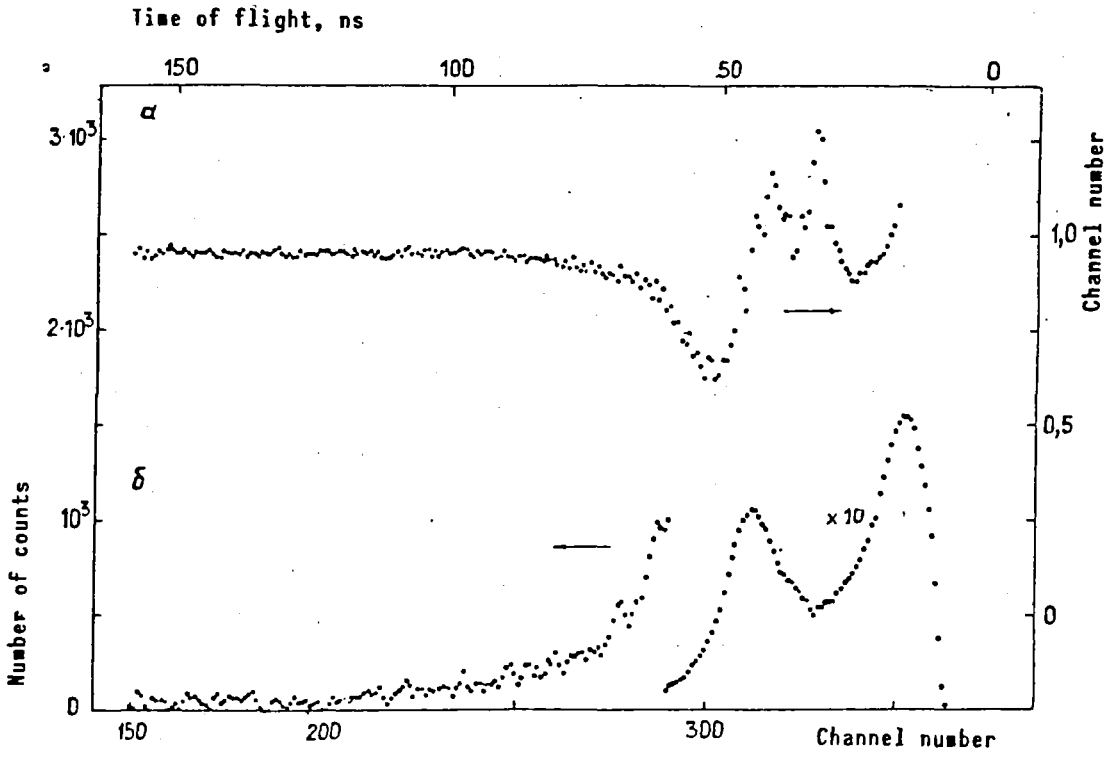

Fig. 5: a - Correction for the difference between a realistic spectrometer response function and a δ-function.

b - Neutron spectrogram P(t).

After this the distribution of P(t) (Fig. 5) was corrected to take account of the difference between a realistic spectrometer response function and the δ-function, in accordance with the expression $P'(t) = \alpha(t)P(t)$. The correction factor $\alpha(t)$ required for this purpose was calculated by means of the expression:

$$a(t) = \{\int \delta[t-t(E)]\varepsilon'(E)\phi(E)dE)\}/[\int F(E,t)\phi(E)dE]$$

where $\phi(E)$ is a Maxwellian distribution with a paramater $T = 1.42$, and $\varepsilon'(E)$ is the theoretical efficiency of the neutron detector calculated on the basis of the formula $\varepsilon'(E) = \int F'(E,t)dt$, where $F'(E,t)$ is the probability of recording at instant t of neutrons emitted from the source with energy E and travelling towards the detector and back within the solid angle of detection Ω - with allowance for possible scattering on isotopes present in the lithium glass, and assuming that both the source and detector were in a vacuum. The realistic spectrometer response function F(E,t) was calculated using the expression $F(E,t) = \int F''(E,t')F'(t,t')dt'$. Here $F''(E,t)$ is

identical to F'(E,t), except that real experimental conditions were assumed for both source and detector; F'(t,t') is the instrument portion of the response function, characterizing the time scatter that occurs when fission products and products of the $^{6}Li(n,\alpha)^{3}H$ reaction are recorded by appropriate detectors and electronics. The distribution of F'(t,t') was obtained using the expression $F'(t,t') = \int F_f(t,t'')F_n(t',t'')dt''$ where $F_f(t,t'')$ and $F_n(t',t'')$ are the instrument response functions of the fast channels of the fission fragment and neutron detectors, respectively (see Fig. 3).

The functions F'(E,t) and F''(E,t) were calculated by the Monte Carlo method. The main characteristics of the models used, were as follows. The zone radius was kept constant (r = 2.25 cm); in calculating the functions F'(E,t) and F''(E,t), the densities of ^{6}Li, ^{7}Li, oxygen and silicon nuclei in zone 10 were taken (for lithium glass thickness k = 0.95 cm) to be 175.4, 8.6, 477.8 and 191.2 nuclei/cm^3 (x 10^{20}) respectively; zones 1, 3, 5, 7, 9 and 11 (h = 100, 1.75, 0.15, 1.87, 27.64 and 100 cm respectively) with oxygen and nitrogen nuclear densities of 0.12 and 0.42 x 10^{20}/cm^3, and zones 2, 4, 6 and 8 (h = 0.01 cm) with a density of iron nuclei of 8.5 x 10^{20}/cm^3 were taken into account only in the calculation of F''(E,t). The neutron source was located on the dividing line between zones 5 and 6. The density of ^{6}Li in the NE-912 lithium glass was calculated from data in the Nuclear Enterprises Ltd Catalogue [10]. The densities of ^{7}Li, oxygen, and silicon nuclei were calculated according to the data given in Ref. [14]. Information on ^{6}Li neutron cross-sections were taken from the ENDF/B-V file, for ^{7}Li, silicon, oxygen and nitrogen from the ENDF/B-IV file, and for iron from Ref. [15]. It was assumed that neutrons were recorded only as a result of the $^{6}Li(n,\alpha)^{3}H$ reaction. Calculations were performed with the BRAND program [16] for 200 energy values ($0 < E_n < 1.5$ MeV) from a monoenergetic neutron source. The results of these calculations are shown in Fig. 3 [functions F''(E,t) for neutron energy values 0.025, 0.245, 0.445 and 1.220 MeV].

The results of applying the correction factor $\alpha(t)$ are shown in Fig. 5a, where we see that the difference between the realistic spectrometer response function and the δ-function is substantial: disregard of it would not only give too soft a spectrum but would also lead to powerful oscillations at the strong lithium and oxygen resonances (0.242 and 0.442 MeV, respectively). In particular, a widening of the spectrometer response function towards longer times owing to preliminary scattering of neutrons at the oxygen resonance of 0.442 MeV can cause a gap in the spectrum of up to 25% at this energy level (see Fig. 5).

Certain simplifications were made in order to speed up calculation of the $F''(E,t)$ functions. In particular, the mixture of gases in the fission chamber was approximated by air, and data for iron were used in place of the data for stainless steel. The 0.08 mm thick aluminium foil which served as detector inlet window was neglected in the calculations. An assessment of the errors which these simplifications could introduce showed them to be relatively small - within the statistical accuracy of the Monte Carlo calculations (i.e. $< 0.5\%$).

After applying the correction factor $\alpha(t)$, the distribution $P'(t)$ was converted into an energy distribution $P(E)$ by a grouping method. For this purpose, values of $P(E)$ were calculated by means of the equation:

$$P(E) = P'_j(t)[j+1-(t_j/\tau)] + \sum_{i=j+1}^{k} P'_i(t) + P'_k(t)[(t_k/\tau)-k]$$

where j = entier (t_j/τ) and k = entier (t_k/τ) are the numbers of time distribution channels, τ is the channel width, t_j and t_k correspond to the boundaries of the energy interval $E - \Delta E/2$ and $E + \Delta E/2$ and are determined by the expression $t = 21.69/\sqrt{E}$, where t is in nanoseconds and E is in megaelectron volts. The advantage of this over the traditional point transformation method is that it permits an energy distribution in equidistant form to be obtained.

To calculate the uncertainty arising from the application of a correction factor for the difference between the realistic spectrometer distribution function and the δ-function, calculations of $\alpha_i(t)$ were made for two Maxwellian distributions of $\phi_i(E)$ with parameters $T_1 = 1.2$ MeV and $T_2 = 1.6$ MeV. Conversion of the distributions $\alpha_i(t)P(t)$ to an energy scale gave two energy distributions for $P_i(E)$, the corresponding systematic error being taken as the energy dependence:

$$D_\alpha^2 = \sum_{i=1}^{2} [1-P_i(E)/\bar{P}(E)]^2$$

where $\bar{P}(E) = 0.5[P_1(E) + P_2(E)]$. Data on D_α are given in the table.

Spectrum of prompt neutrons from spontaneous fision of ^{252}Cf N(E), Neutron recording efficiency ε(E), and Relative errors in these quantities.

E, keV	N(E)x10², neutrons·fiss⁻¹·MeV⁻¹·sr⁻¹	ε(E), %	$D_{st\ N}$, %	D_α, %	D_ε, %	D_N, %
25	3,27	1,89	13,15	0,03	2,94	13,56
35	2,72	1,70	15,80	0,04	2,94	16,15
45	4,34	1,53	10,14	0,03	2,95	10,67
55	4,37	1,39	10,30	0,03	2,96	10,83
65	4,55	1,35	9,45	0,03	2,96	10,02
75	5,05	1,29	8,61	0,05	2,97	9,15
85	4,89	1,29	8,18	0,06	2,97	8,84
95	5,67	1,32	6,53	0,07	2,97	7,34
105	5,67	1,34	6,00	0,08	2,97	6,88
115	6,44	1,38	4,81	0,10	5,46	7,44
125	7,35	1,40	3,95	0,12	5,46	6,92
135	7,12	1,48	3,51	0,15	5,46	6,68
145	6,86	1,58	3,21	0,20	5,46	6,53
155	7,83	1,74	2,55	0,22	5,45	6,23
165	7,72	1,94	2,33	0,24	5,45	6,14
175	7,05	2,65	1,99	0,25	5,45	6,01
185	8,39	2,62	1,67	0,25	5,44	5,91
195	7,38	3,78	1,49	0,26	5,44	5,86
205	7,12	4,58	1,26	0,25	5,44	5,80
215	8,39	5,38	1,07	0,23	5,43	5,76
225	8,02	5,40	1,12	0,23	5,43	5,77
235	7,76	6,52	1,03	0,23	5,43	5,75
245	7,83	6,54	1,02	0,20	5,43	5,74
255	8,02	5,72	0,99	0,20	5,43	5,74
265	8,95	5,00	0,78	0,21	5,44	5,71
275	8,47	5,16	1,06	0,22	5,44	5,76
285	8,35	4,54	1,20	0,25	5,44	5,79
295	9,55	3,35	1,26	0,26	5,45	5,81
305	9,21	2,97	1,41	0,29	5,45	5,85
315	9,19	2,70	1,52	0,32	5,46	5,88
325	8,64	2,69	1,50	0,26	5,46	5,88
335	9,38	2,19	1,60	0,36	5,46	5,91
345	8,88	2,04	1,80	0,38	5,46	5,97
355	9,32	1,88	1,82	0,40	5,47	5,99
365	9,14	1,89	1,86	0,42	5,47	6,00
375	9,17	1,79	1,96	0,42	5,47	6,03
385	9,40	1,62	2,02	0,45	5,47	6,05
395	9,06	1,59	2,10	0,46	5,47	6,02

Continued

E, keV	N(E)x10^2, neutrons-fiss^{-1}·MeV^{-1}·sr^{-1}	ϵ(E), %	$D_{st\ N}$, %	D_α, %	D_ϵ, %	D_N, %
410	9,70	1,48	1,55	0,49	5,44	5,69
430	9,99	1,36	1,60	0,53	5,44	5,90
450	9,43	1,28	1,70	0,60	5,44	5,94
470	9,73	1,11	1,95	0,65	5,44	6,02
490	9,39	0,99	1,92	0,75	5,44	6,04
510	9,86	0,89	1,93	0,80	5,43	6,03
530	10,14	0,82	1,97	0,90	5,43	6,05
550	10,03	0,76	2,09	0,92	5,43	6,10
570	9,67	0,74	2,17	1,05	5,43	6,14
590	9,85	0,71	2,13	1,13	5,44	6,15
610	10,10	0,68	2,18	1,20	5,44	6,18
630	10,03	0,65	2,19	1,25	5,44	6,20
650	10,07	0,63	2,28	1,32	5,44	6,24
670	10,03	0,62	2,29	1,38	5,44	6,28
690	9,99	0,60	2,30	1,45	5,44	6,28
710	10,37	0,56	2,31	1,50	5,45	6,30
735	10,41	0,54	1,92	1,57	5,44	6,18
765	10,55	0,52	1,89	1,63	5,44	6,18
795	10,22	0,53	1,96	1,70	5,45	6,23
825	9,99	0,54	2,00	1,76	5,44	6,26
855	9,66	0,54	1,97	1,80	5,45	6,27
855	10,07	0,53	1,99	1,85	5,45	6,29
915	9,73	0,53	2,06	1,87	5,45	6,32
945	9,70	0,53	2,06	1,91	5,45	6,33
975	9,47	0,54	2,01	1,96	5,46	6,34
1005	9,51	0,54	2,00	2,01	5,46	6,35
1020	9,40	0,53	1,81	2,01	5,45	6,28
1060	10,03	0,52	1,69	1,97	5,45	6,24
1100	10,00	0,50	1,80	1,90	5,46	6,25
1140	10,07	0,51	1,69	1,80	5,46	6,19
1180	9,66	0,50	1,76	1,80	5,46	6,21
1220	10,00	0,50	1,80	1,61	5,46	6,17

Note: $D_{st\ N}$ is the statistical error of the measurement; D_α is the energy-dependent systematic error; D_ϵ is the total error in the neutron recording efficiency; and D_N is the total error in the measurement.

Neutron detection efficiency

The efficiency of the NE-912 thick lithium glass used in this experiment was experimentally determined. The methods of measurement, treatment of experimental data, and the results obtained are explained in reasonable detail in Refs [11, 17]. Measurements of the efficiency of the NE-912 glass were performed with reference to the thin (0.0835 cm) NE-908 glass. The efficiency of the NE-908 glass, in turn, was calculated with the BRAND progam [16]. The calculation model (except for zone 10) was similar to that described above for calculation of the function F'(E,t). The thickness of zone 10 and the densities of ^{6}Li, ^{7}Li, silicon and oxygen nuclei in it were taken to be 0.0835 cm, and 172.4, 8.0, 182.1 and 487.3 (x 10^{20}) nuclei/cm^3. The density of ^{6}Li nuclei was taken as given in Ref. [11]:

$n_o x = (1.44 \pm 0.03) \times 10^{21}$ nuclei/cm^3. The densities of ^{7}Li, silicon and oxygen nuclei were taken from Ref. [18]. The table shows data for the efficiency of the NE-912 lithium glass, obtained by normalizing the experimental data of Ref. [11] to the new calculated efficiency of the NE-908 thin lithium glass. The total error in the neutron detection efficiency of the NE-912 glass is also given. This error was calculated from the formula $D_\varepsilon^2 = D_{st}^2 + D_{calc}^2$ where D_{st} is the relative statistical error in the experimental data, varying between 0.5 and 0.9%, depending on the energy of the neutrons detected; $D_{st\ M-K}$ (= 0.5%) is the relative statistical accuracy of the Monte Carlo calculations; D_{calc} is the relative error in calculating the efficiency of the NE-908 glass:

$$D_{calc}^2 = D_{st\ M-K}^2 + D_\rho^2 + D_\sigma^2,$$

where D_ρ (= 2%) is the relative error in measuring a density of nuclei ρ in the thin lithium glass; and D_σ is the relative accuracy of the cross-section data for the ^{6}Li(n,α)^{3}H reaction (this was taken to be $\pm$ 2% for the energy region < 100 keV and $\pm$ 5% for higher energies).

Discussion of results

The spectrum of ^{252}Cf prompt spontaneous fission neutrons was obtained with the expression $N(E) = P(E)/N_f\Omega_\varepsilon(E)$, where N_f is the number of fission events. Numerical data for this spectrum are given in the table. The total error in measuring this spectrum, D_N, was calculated on the assumption that all errors considered are independent. If this is so, then:

$$D_N^2 = D_{st\ N}^2 + D_\alpha^2 + D_\varepsilon^2 + D_\Omega^2 + D_{N_f}^2.$$

Figure 6 shows the relationship of the experimental data to a Maxwellian distribution with parameters $\bar{\nu}_p$ = 3.757 (ENDF/B-V) and T = 1.42 MeV:

$$M(E) = \frac{\bar{\nu}_p}{2\Pi^{3/2}\ T^{3/2}} \sqrt{E_n} \exp(-E_n/T).$$

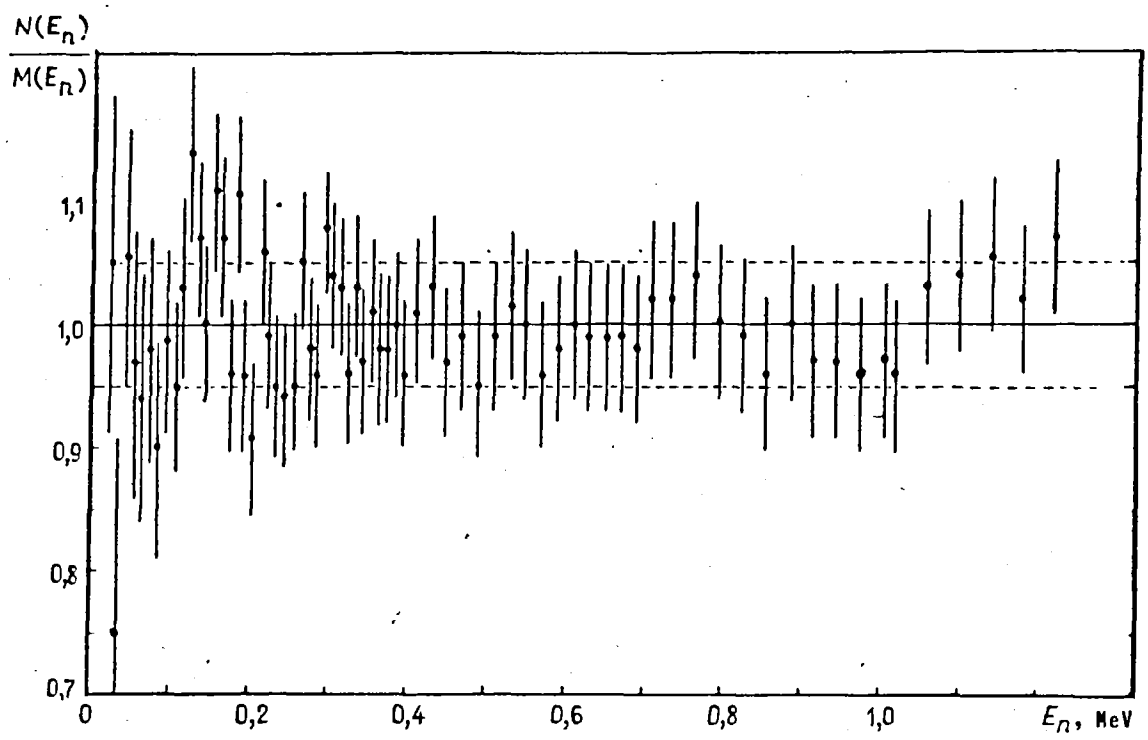

Fig. 6: Relationship of the experimental results obtained in this paper to a Maxwellian distribution.

It will be seen that a Maxwellian distribution with these parameters satisfactorily describes the results obtained. With the exception of a few points, the deviation of the experimental data from the corresponding values of the Maxwellian distribution does not exceed $\pm$ 5%.

In conclusion, we should note that the measurements reported in this paper are absolute measurements in the sense that there was no fitting either to $\bar{\nu}_p$ or to the hard portion of the spectrum. The only reference qunatity used in processing the data was the energy dependence of the $^6Li(n,\alpha)^3H$ reaction cross-section, which has been studied quite thoroughly and constitutes an international standard.

PROMPT NEUTRON SPECTRA FROM FISSION OF ^{233}U, ^{235}U AND ^{239}Pu BY THERMAL NEUTRONS AND FROM SPONTANEOUS FISSION OF ^{252}Cf IN THE 0.01-12 MeV ENERGY RANGE

B.I. Starostov, V.N. Nefedov, A.A. Bojtsov

Although a substantial amount of experimental data on prompt neutron spectra for fission of ^{233}U, ^{235}U and ^{239}Pu by thermal neutrons and for spontaneous fission of ^{252}Cf has been accumulated, the results of work in recent years show a considerable spread, particularly in the neutron energy regions below 1 and above 5 MeV. In our work, the prompt fission neutron spectra given were measured using the same spectrometer over a broad range of energies, 0.01-12 MeV (in which 99.9% of all neutrons lie); this was done in two cycles which differed in the methods used to record neutrons and fission fragments.

Measurement method and basic calculation relationships. The prompt fission neutron spectra were measured using the time-of-flight method. The neutron energies were determined by the formula:

$$E = 9.3449 \cdot 10^2 \left[(1-0.212882 \cdot 10^{-2}E')^{-1/2}-1\right]. \quad (1)$$

Here E' is the neutron energy in a non-relativistic approximation (in MeV):

$$E' = (72.288\ L/t)^2, \quad (2)$$

where L is the flight distance in m, and t is the flight time of the neutron over the distance L, in ns.

The time spectra were transformed into energy spectra by the formula:

$$n(E) = n(E')2(1-0.212882 \cdot 10^{-2}E')^{3/2}/9.3449 \cdot 0,\ 212882. \quad (3)$$

Here n(E) is the intensity of the spectrum (number of neutrons with energy E in a unit range of energies in MeV, normalized for a single fission event and a solid angle of 4π steradians):

$$n(E') = \frac{N(t)t^3}{(72.288)^2\ 2L^2(\Omega/4\pi)n_{fiss.}\tau\xi(E)}, \quad (4)$$

Table 1. Characteristics of the neutron spectrometer.

Characteristics	Measurement cycle				
	First			Second	
Type	With anthracene	With stilbene	With plastic	GSID[*]	Ionization chamber
Flight path, cm	51	231,3	611	10,4; 21,4; 29,5	12,4; 21,4; 40
Time width of the analyser channel, ns	1,423±0,002	1,3938±0,0014	1,4142±0,0014	0,734±0,002	0,595±0,001
Time resolution, ns	4,2	4,2	4,2	2,5	4,5

Note: In all cases, the error in the "zero" time position is 0.25 ns.
[*] Gas scintillation ionization detector.

Table 2. Characteristics of the fragment detector.

Characteristics	Measurement cycle	
	First	Second
Type	MIC[*]	GSD[**]
Material	Stainless steel	Aluminium
Backing sheet, cm:		
thickness	0,005	0,0003
radius	1,25	—
dimensions	—	3,8x3,8 cm^2
Number of fission events recorded, fiss./s x 10^5	0,7	1,2; 2
Fragment recording efficiency, %	98	97
Angle between target plane and neutron detector	0^o; 45^o	0^o

[*] Miniature ionization chamber.
[**] Gas scintillation detector.

Table 3. Characteristics of the neutron detector.

Characteristics	Measurement cycle				
	First			Second	
Type	With anthracene	With stilbene	With plastic	GSID[*]	IC[**]
Height, cm	0,4	3	12	0,01	0,8
Diameter, cm	1,8	7	20	11	10
Energy range, MeV	0,1—2	1,4—8	3—12	0,01—5	0,01—5
Partial error, $\Delta\xi/\xi$, %	2,5	Reference error		$\Delta\sigma_{n,f}/\sigma_f$	$\leq$ 4%

[*] Gas scintillation ionization detector.
[**] Ionization chamber.

where N(t) is the number of neutrons recorded over a flight time t; $\Omega/4\pi$ is the solid angle subtended by the detector as seen from the fissioning nuclide target; $n_{fiss.}$ is the true number of fission events recorded; τ is the time width of the analyser channel; and $\xi(E)$ is the recording efficiency for a neutron with energy E.

Neutron spectrometer (Table 1). Fission fragment detectors were used to determine the neutron emission time (Table 2), and neutron detectors to determine the time of recording (Table 3).

In the first measurement cycle, four identical miniature ionization chambers were used to record the fragments, each ionization chamber having a target of the corresponding nuclide. The mass of each stainless steel chamber did not exceed 2.5 g. The nuclide targets were applied to an electropolished stainless steel backing. The miniature ionization chambers were filled with purified methane to a pressure of 1×10^5 Pa. The fragment recording efficiency ξ_f was 99% for the ^{252}Cf targets and 98% for the ^{233}U, ^{235}U and ^{239}Pu targets. Three scintillation-type neutron detectors were used: in this cycle to measure the prompt fission neutron spectrum in the 0.1-12 MeV energy range with an energy resolution of about 5% and a statistical error of 1-2%. The first detector (see Table 3), based on the FEhU-71 photomultiplier, with a mass of 35 g and an anthracene crystal 1.8 cm in diameter and 0.4 cm high, had a low neutron recording threshold (about 20 keV) and was used to measure the spectra in the 0.08-2 MeV energy range at a flight distance of 51 cm. Steps were taken to reduce the mass of the detector components in order to diminish the background of scattered neutrons. The second detector, based on the FEhU-63 photomultiplier and a stilbene crystal 7 cm in diameter and 3 cm high, was used for measurements at a flight distance of 231.3 cm in the 1.4-8 MeV neutron energy range. The third detector, based on the same photomultiplier and a plastic crystal 20 cm in diameter and 12 cm high, was used for measurements at a flight distance of 611 cm in the 3-12 MeV energy range.

In the second measurement cycle, gas scintillation fission fragment detectors were used together with thresholdless neutron detectors: ionization chambers with layers of ^{235}U and a gas scintillation ionization detector with a metallic ^{235}U radiator [1, 2]. The measurements were made in the 0.01-5 MeV energy range. For the measurements of the ^{252}Cf spectra, an ionization chamber with "thin" walls similar to that described in Ref. [2], but with a mass of 65 g (one order of magnitude less), was used. This chamber was developed in accordance with the recommendations of the authors of Ref. [3]. It has eight layers of ^{235}U on four backing sheets. The height of the assembly of ^{235}U layers was 0.8 cm (see Table 2).

The fragment detectors were placed in the beam of thermal neutrons and γ-quanta in a horizontal channel of the SM-2 reactor, the neutron detectors in the protection equipment [2]. The block diagram for the electronic apparatus represented a conventional fast-slow coincidence circuit.

Data processing. The methods described in Refs [2, 4] were used to determine the flight distances, the solid angles, the numbers of recorded neutrons and fission events, the time width of the channel, the time resolution and the "zero" time position. The effect of anisotropy of the fission fragment recording was investigated by measuring the prompt fission neutron spectra at angles of 0°, 45° and 90° to the target planes and calculating their relationship. It was established that this effect could be neglected in these measurements. The time spectra obtained after background subtraction were transformed into equipment energy spectra N(E) using formulae (1)-(4), on the assumption that the efficiency $\xi = f(E) = 1$. Calculated corrections were made to these spectra for the background of neutrons scattered by the target backing, in the gas, by the walls of the miniature ionization chambers and gas scintillation detectors, by atoms in the air at an angle Ω, by the lead shielding the scintillation detectors from delayed γ-quanta, and by all the components of the neutron detectors. At this stage in the processing of the data, we obtained intensity ratios for the

Table 4. Averaged data on prompt fission neutron spectra for ^{252}Cf.

E, MeV	ΔE, MeV	$n(E)/n_M(E)$ (T = 1,42 MeV)	δ, %	E, MeV	ΔE, MeV	$n(E)/n_M(E)$ (T = 1,42 MeV)	δ, %
0,0003	0,0001	1,084	40	2,123	0,031	1,023	2
0,0007	0,0002	1,084	30	2,216	0,031	1,027	1,5
0,0015	0,0004	0,958	20	2,314	0,031	1,024	1,5
0,0025	0,0003	0,958	15	2,400	0,031	1,030	1,5
0,0034	0,0003	0,972	10	2,537	0,038	1,034	2
0,0044	0,0003	0,972	10	2,662	0,033	1,030	2,2
0,0055	0,0003	0,957	9	2,772	0,03	1,034	2,5
0,0065	0,0003	0,955	8	2,875	0,041	1,026	2,6
0,0075	0,0003	0,983	8	2,964	0,031	1,034	2,2
0,0084	0,0004	0,983	8	3,151	0,034	1,020	2
0,0095	0,0006	0,975	7	3,305	0,033	1,024	2,5
0,0154	0,0026	0,973	7	3,408	0,062	1,015	2,3
0,0344	0,0021	0,965	7	3,537	0,062	1,015	2,3
0,060	0,002	0,971	6	3,629	0,068	1,014	2,3
0,081	0,003	0,988	5	4,155	0,062	1,015	2,5
0,091	0,003	1,000	4	4,268	0,062	1,015	2,5
0,104	0,003	1,028	3	4,398	0,065	1,017	2,3
0,115	0,003	1,026	3	4,582	0,065	1,015	2,5
0,134	0,003	1,010	2,5	4,777	0,065	1,015	2
0,144	0,003	1,018	2,5	4,986	0,065	1,013	2
0,803	0,007	0,973	2	5,208	0,065	1,018	2
0,868	0,009	0,978	2	5,446	0,065	1,011	3
0,155	0,003	0,999	2,5	5,700	0,065	0,999	4
0,166	0,003	0,983	2,5	5,973	0,065	0,993	4
0,178	0,003	0,970	2,5	6,170	0,15	0,989	4
0,194	0,004	0,962	2,5	6,270	0,15	0,988	4
0,207	0,004	0,964	2,5	6,370	0,16	0,988	4
0,221	0,004	0,968	2,5	6,470	0,16	0,989	4
0,239	0,005	0,975	3	6,580	0,16	0,987	4
0,263	0,006	0,974	3	6,69	0,16	0,985	4
0,287	0,006	0,989	3	6,81	0,16	0,989	5
0,320	0,006	0,982	3	6,92	0,16	0,986	5
0,430	0,007	0,989	3	7,04	0,16	0,986	5
0,357	0,008	0,988	2	7,16	0,16	0,984	5
0,382	0,008	0,982	2	7,29	0,16	0,980	5
0,427	0,008	0,989	2	7,42	0,20	0,974	5
0,456	0,008	0,973	2	7,55	0,20	0,864	5
0,499	0,008	0,976	2	7,68	0,20	0,959	5
0,549	0,008	0,979	2	7,82	0,20	0,952	5
0,631	0,006	0,962	2	7,97	0,20	0,950	5,5
0,692	0,006	0,976	2	8,11	0,20	0,949	5,5
0,737	0,006	0,977	2	8,27	0,20	0,946	6
3,748	0,068	1,014	2,3	8,42	0,20	0,943	6
3,938	0,062	1,017	2,3	8,58	0,20	0,941	6
0,906	0,011	1,000	2	8,75	0,20	0,932	6
1,002	0,028	0,996	2	9,92	0,20	0,927	6
1,050	0,028	1,002	2	9,09	0,20	0,923	6
1,170	0,028	1,011	2	9,46	0,20	0,915	6,5
1,260	0,029	1,023	3	10,0	0,20	0,906	6,5
1,353	0,035	1,028	2,5	10,7	0,20	0,873	7
1,480	0,029	1,044	2,5	11,3	0,20	0,850	7
1,640	0,026	1,026	2,5	11,9	0,20	0,838	7
1,760	0,025	1,020	2,5	12,5	0,20	0,831	8
1,836	0,026	1,027	2	13,6	0,2	0,789	9
1,990	0,030	1,024	2	15,4	0,3	0,772	10

equipment energy prompt fission neutron spectra for $^{252}Cf/^{239}Pu$, $^{252}Cf/^{235}U$ and $^{252}Cf/^{233}U$ in the 0.01-12 MeV energy range, independently of systematic errors in determining the efficiency $\xi(E)$.

In order to obtain data on the prompt fission neutron spectra themselves, it is necessary to know the efficiency of the neutron detectors.

In the first measurement cycle, absolute efficiencies $\xi = f(E)$ were calculated from data on the neutron cross-sections for elastic scattering by hydrogen nuclei. Analysis of the results of the efficiency calculations by the Monte-Carlo method [5] shows that in many cases only double scattering of neutrons by hydrogen nuclei need be taken into account, since triple and quadruple scattering make a negligible contribution to the efficiency. These calculations showed that the flux depression effect in the scintillator due to scattering of neutrons by carbon nuclei is compensated by the effect of double processes, in which the neutron is first scattered by a carbon nucleus and then by a proton. In this case, the efficiencies $\xi = f(E)$ were calculated taking into account double scattering of neutrons by hydrogen nuclei, the non-linearity of the scintillators' light output, and the neutrons and γ-quanta produced by the $^{12}C(n,n')$ and $^{12}C(n,n'\gamma)$ reactions, as well as the contribution of neutrons scattered by the photomultiplier, with corrections for their time shift.

The counting energy threshold B (minimum energy at which neutrons start to be recorded) was determined experimentally from the equipment energy prompt fission neutron spectra. In the spectral region N(E), where the effect of the pulse discrimination level was apparent, a straight line was fitted to the spectrum by the least-squares method; its point of intersection with the E axis gave the value of B. The main measurements were made at the thresholds shown in Fig. 1.

The calculated efficiencies were used only in the case of the anthracene detector, since the contribution to the efficiency of double scattering of neutrons by hydrogen nuclei and the background of neutrons scattered by the photomultiplier together did not exceed 3%, and the energy threshold was determined with an error of 1 keV. The calculated error of the dependence $\xi = f(E)$ obtained was evaluated as 2.5%. The anthracene neutron detector was used to make absolute measurements, i.e. measurements to determine all the constants from formulae (1)-(4) and the prompt fission

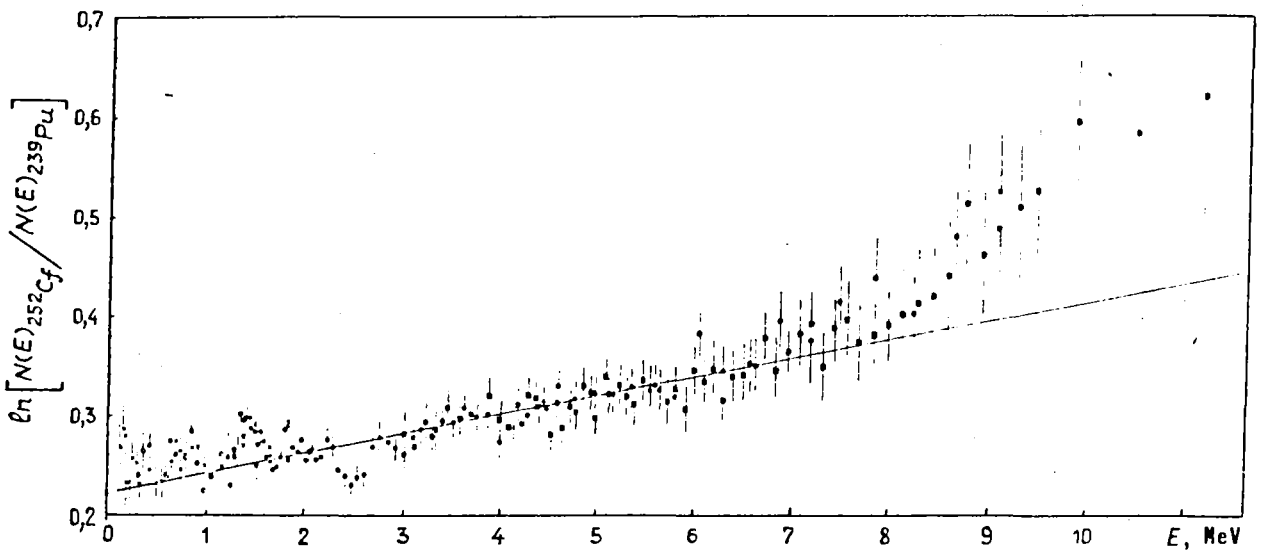

Fig. 1. Ratios of the equipment energy prompt fission neutron spectra for $^{252}Cf/^{239}Pu$ from measurements (first cycle) using an anthracene detector, L = 51 cm ($\dagger$ - B = 0.0214 MeV; ϕ - B = 0.128 MeV), stilbene detector, L = 231.3 cm (ϕ - B = 0.886 MeV); plastic detector, L = 611 cm (Φ - B = 2.498 MeV); —— - ratio of distributions (5) for ^{252}Cf with a spectral "hardness" parameter T = 1.42 MeV, $\bar{\nu}_f$ = 3.76 and for ^{239}Pu with T = 1.382 MeV, $\bar{\nu}_f$ = 2.89. The errors are statistical.

neutron spectra for ^{252}Cf, $^{233}U + n_T$, $^{235}U + n_T$, and $^{239}Pu + n_T$ in the 0.08-2 MeV energy range. The efficiencies of the stilbene and plastic detectors were determined on the basis of assumptions about the initial shape of the ^{252}Cf spectra; the results of weighted averagings performed by the method described in Ref. [6] were taken for the initial spectrum. In the 0.01-2 MeV range, the results from Refs [7-9] and our own work were given the main weight in the average. For the 2-15 MeV range, we drew both on work analysed earlier [6] and on more recent work [8, 10-14]. The averages are given in Table 4, in the form of ratios of the intensities n(E) to the intensities $n_M(E)$ of a Maxwellian distribution.

$$n_M(E) = C\, E^{1/2} \exp(-E/T), \qquad (5)$$

where C is a constant; T is the "hardness" parameter of the spectrum (for the ^{252}Cf spectrum, T = 1.42 MeV). In the 2-12 MeV range, the averages agree with the evaluation of the ^{252}Cf spectrum in Ref. [15]. The stilbene and plastic detectors were used to obtain the prompt fission neutron spectra for $^{233}U + n_T$, $^{235}U + n_T$ and $^{239}Pu + n_T$ with respect to the averaged

data on the ^{252}Cf spectra in the 2-12 MeV energy range. However, for all the scintillation detectors and selected energy thresholds, agreement to within 3% was achieved between the calculated efficiencies and the efficiencies obtained on the basis of the averaged data on the ^{252}Cf prompt fission neutron spectra.

In the second cycle of measurements of the prompt fission neutron spectra for ^{252}Cf in the 0.01-5 MeV range, the efficiency $\xi = f(E)$ of the ionization chamber and gas scintillation ionization detectors was taken to be proportional to the fission cross-sections for ^{235}U evaluated in Ref. [16]. The measurements of the spectra for $^{233}U + n_T$, $^{235}U + n_T$ and $^{239}Pu + n_T$ were made relative to the averaged data on ^{252}Cf spectra owing to the difficulties of taking into account the background of neutrons scattered by the protection equipment and components of the gas scintillation ionization detector and ionization chambers. The intensities of the prompt fission neutron spectra were obtained in relative units in this cycle.

After introducing in formula (4) the values of $\xi = f(E)$, we obtained the prompt fission neutron spectra without taking the time resolution of the spectrometer into account. The resolution was taken into account on the basis of the assumed shape of the spectra in the form of a Maxwellian distribution [17]. The corrections for the resolution did not exceed $\pm$ 1.5%.

All the data from the second measurement cycle were normalized with respect to the data from the first cycle, and in the 0.01-12 MeV energy range, the mean energies of the prompt fission neutron spectra were calculated from the formula:

$$\bar{E} = \int_0^\infty En(E)dE / \int_0^\infty n(E)dE. \qquad (6)$$

The errors in the values of $\bar{E}$ were found from its changes during change in n(E) and E within the limits of the total measurement errors. In order to determine the total errors on the basis of formulae (1)-(4), a list of some 20 partial errors was drawn up. A significant contribution to the total error of n(E) was made by the partial error $\Delta\xi/\xi$.

Measurement results and discussion. For the ^{252}Cf, $^{233}U + n_T$, $^{235}U + n_T$ and $^{239}Pu + n_T$ spectra, mean energies of 2.134 ± 0.015; 2.015 ± 0.015; 1.970 ± 0.015 and 2.087 ± 0.015 MeV, respectively, were obtained by formula (6). The parameters T of the Maxwellian distribution were determined from the relationship $\bar{E} = (3/2)T$. For the ^{252}Cf, $^{233}U + n_T$, $^{235}U + n_T$ and $^{239}Pu + n_T$ spectra, the parameters T were taken to be 1.42; 1.34; 1.313 and 1.382 MeV, respectively.

Figure 1 shows measurement results for the $^{252}Cf/^{239}Pu$ spectrum intensity ratios; similar information was obtained in measuring the ratios for $^{235}Cf/^{235}U$ and $^{252}Cf/^{233}U$. These data were used to check the data for each spectrum against the body of data for other spectra. In particular, data on the ^{252}Cf spectra in the 5–10 MeV energy range were obtained from the $N(E)_{^{252}Cf}/N(E)_{^{239}Pu}$ ratio on the assumption that the $^{239}Pu + n_T$ spectrum is described by the results of averaging the data from Ref. [6]. From the prompt fission neutron spectra intensity ratios, it was established that:

- The results of the first and second measurement cycles in the energy range covered by the data (0.1–5 MeV) agree;
- The ratios in the 0.01–7.5 MeV range generally agree with the intensity ratios of the corresponding distributions (5);
- In the 7.5–12 MeV range, the intensity ratios of the prompt fission neutron spectra are greater than the intensity ratios of the distributions (5).

The discrepancies between the intensity ratios of the prompt fission neutron spectra and the intensity ratios of the corresponding distributions (5) in the 7.5–12 MeV range show that the prompt fission neutron spectra in the range $E \geq 7.5$ MeV cannot be described by distribution (5). Furthermore, the discrepancies between the prompt fission neutron spectra themselves and distribution (5) are different for fission of ^{252}Cf and of other nuclides. The spectral ratios obtained with the best statistical accuracy were those for ^{252}Cf and ^{239}Pu. These ratios show an interesting

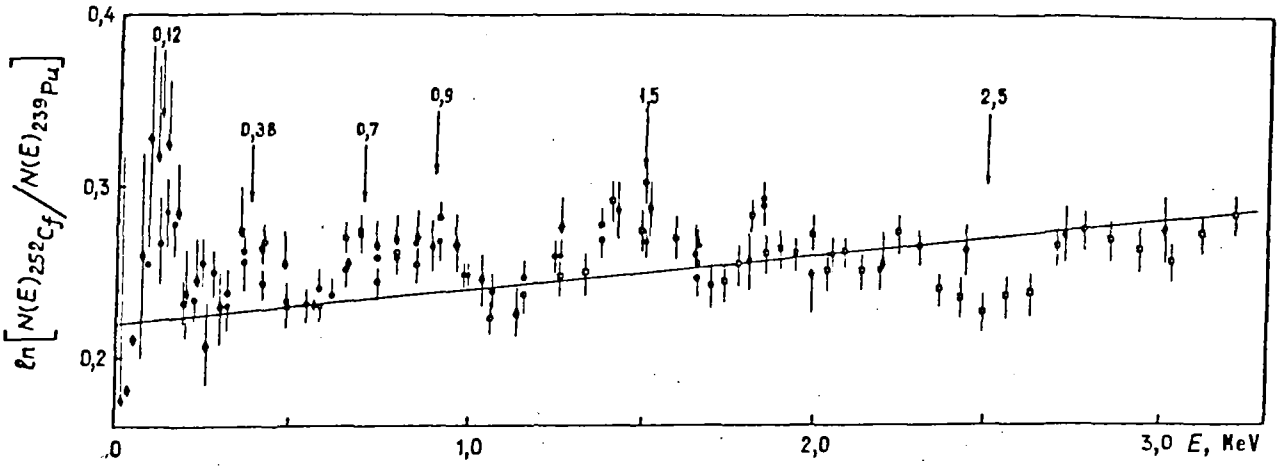

Fig. 2. Ratio of the equipment energy prompt fission neutron spectra for $^{252}Cf/^{239}Pu$. Data from the first measurement cycle: ϕ - L = 51 cm, B = 0.0214 MeV; ϕ - L = 51 cm, B = 0.128 MeV; ϕ - L = 231.3 cm, B = 0.886 MeV, ϕ - data from the second measurement cycle; —·- ratio of distribution (5) for ^{252}Cf with parameters T = 1.42 MeV, $\bar{\nu}_f$ = 3.76 and for ^{239}Pu with T = 1.382 MeV, $\bar{\nu}_f$ = 2.89.

pattern in the 0.1–2 MeV energy range: for certain neutron energies, irregularities are observed which exceed the ratios of distributions (5) on average by 4%.

The fragment of $N(E)_{^{252}Cf}/N(E)_{^{239}Pu}$ ratios in the 0.01–3 MeV energy range from Fig. 1, together with the ratios from the second measurement cycle, are shown in Fig. 2. The irregularities observed in both measurement cycles which can be seen in this figure generally agree in terms of the neutron energies, although the measurements were carried out under different conditions and with different detectors. These irregularities may occur in the prompt fission neutron spectra themselves, owing to the contribution of neutrons which are resonance scattered by the construction materials of the detectors, in particular by silicon, oxygen, nitrogen and nickel nuclei. However, in these measurements these contributions should compensate each other, since all conditions were the same. Other effects which might cause irregularities, such as the change in the differential linearity of the spectrometer in the measurements of the prompt fission neutron spectra for $^{239}Pu + n_T$ due to charging of the fragment detector by α-particle pulses as compared with the measurements of the ^{252}Cf spectra, or the possible contribution to the $^{239}Pu + n_T$ spectra of neutrons from (α,n) reactions

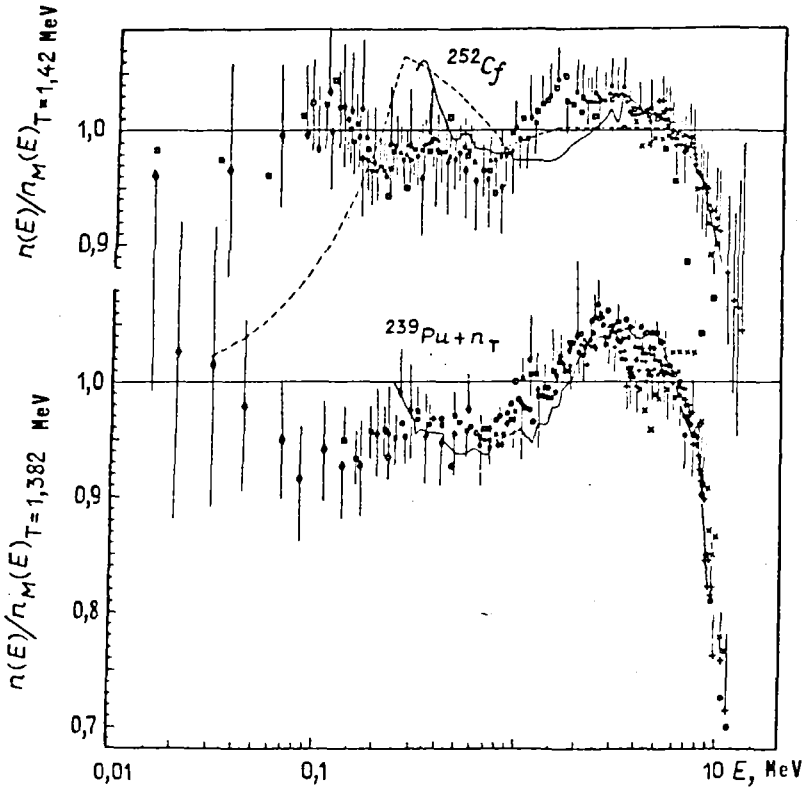

Fig. 3. Ratio of prompt fission neutron spectra for ^{252}Cf and $^{239}Pu + n_T$ to distributions (5): ✱ , ✦ , ⁞ - first measurement cycle; ✦ - second measurement cycle. Evaluations from --- [15]; ____ - [6]. Results of experimental work: □ - [8]; x - [13]; 0 - [19].

are also unlikely. No changes in the differential linearity were detected experimentally. In the measurements made using coincidence methods, including the time-of-flight method, the contribution of (α,n) reactions from α-particles whose pulses were discriminated was completely excluded. Above the discrimination level, the counting rate for α-particles in the case of $^{239}Pu + n_T$ was 5% of the fission fragment counting rate. The neutron yield from the interaction of these recorded α-particles with the material of the detectors is negligible by comparison with the neutron yield during fission of $^{239}Pu + n_T$. Since the irregularities in the data for both measurement cycles agree, it can be assumed that some ^{252}Cf fission fragment nuclei (whose yield is small in the case of $^{239}Pu + n_T$ fission) may possibly emit monoenergetic neutrons - about 1% of all ^{252}Cf fission neutrons.

Figures 3 and 4 show the prompt fission neutron spectra for ^{252}Cf, $^{239}Pu + n_T$, $^{235}U + n_T$ and $^{233}U + n_T$ in the form of ratios of their

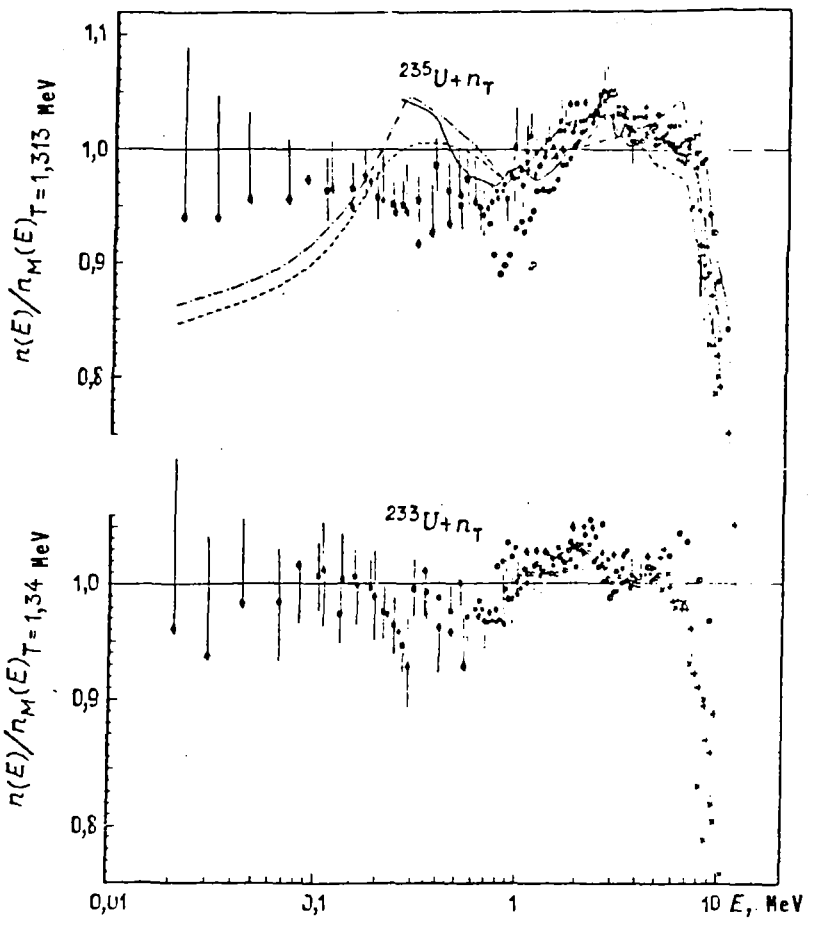

Fig. 4. Ratio of prompt fission neutron spectra for $^{235}U + n_T$ and $^{233}U + n_T$ to distributions (5): ✱, ◆, ╪ - first measurement cycle; ◆ second measurement cycle. Evaluations from -.- - [15]; ——— - [6]; —— - [18] (integral measurement data). Results of experimental work: 0 - [20, 21]; x - [13].

intensities n(E) to the intensities $n_M(E)$ of the corresponding distributions (5). Basic regularities can be seen in the deviations between the prompt fission neutron spectra and the corresponding distributions (5): the intensity of the spectra is several percent lower in the 0.01-1 MeV energy range, higher in the 1-6 MeV range, and substantially lower in the 6-12 MeV range. Also, agreement between the results of the first and second measurement cycles is observed. The reduction in the intensity of the prompt fission neutron spectra in the region above 6 MeV by comparison with distribution (5) can be explained by the "finiteness" of the mean fragment excitation energy. Figures 3 and 4 also show the results of other work and evaluations. They agree with the results of our work, with the exception of Ref. [20] for the spectra of prompt neutrons from fission of ^{235}U by

neutrons with E = 0.5 MeV. In the 0.5-2 MeV energy range, the results of Ref. [20] are erroneous. Calculations of prompt fission neutron spectra from the model in Ref. [22] have shown that it only qualitatively describes the deviations observed between these spectra and distribution (5).

In nuclear reactor calculations group constants for the spectra (Table 5) are used. The difference between the accepted constants and the ones obtained is up to 10%.

Table 5. Group constants for prompt fission neutron spectra.

Group No.	Energy range, MeV	Group constants		
		$^{239}Pu+n_T$	$^{235}U+n_T$	$^{233}U+n_T$
1	6,5—10,5	0,02236	0,01946	0,01944
2	4—6,5	0,09924	0,08779	0,09146
3	2,5—4	0,1894	0,1757	0,1820
4	1,4—2,5	0,2678	0,2623	0,2680
5	0,8—1,4	0,1937	0,2032	0,2003
6	0,4—0,8	0,1321	0,1457	0,1378
7	0,2—0,4	0,05847	0,06475	0,06130
8	0,1—0,2	0,02252	0,02577	0,02481
9	0,0465—0,1	0,00988	0,01036	0,00999
10	0,0215—0,0465	0,00309	0,00342	0,00349
11	0,01—0,0215	0,00144	0,00155	0,00141

From the foregoing, we may draw the following conclusions:

1. The intensity ratios of the equipment energy prompt fission neutron spectra for $^{252}Cf/^{239}Pu$, $^{252}Cf/^{235}U$ and $^{252}Cf/^{233}U$ in the 0.01-7.5 MeV energy range agree with the intensity ratios of the corresponding distributions (5), while in the 7.5-12 MeV range they are greater;
2. For the $N(E)_{^{252}Cf}/N(E)_{^{239}Pu}$ ratios, the results from both measurement cycles revealed some irregularities which exceeded the intensity ratios of distributions (5) on average by 4%;
3. All the measurement results show that there is a definite relationship between the prompt fission neutron spectra and distributions (5);
4. The mean energies of the prompt fission neutron spectra for ^{252}Cf, $^{233}U + n_T$, $^{239}U + n_T$ and $^{239}Pu + n_T$ are

2.134 $\pm$ 0.015; 2.015 $\pm$ 0.015; 1.970 $\pm$ 0.015 and 2.087 $\pm$ 0.015 MeV, respectively;

5. The calculated group constants for the prompt fission neutron spectra differ from the accepted ones by up to 10%. Further research is needed on the effect of the new constants on the calculated characteristics of reactors and critical assemblies.

LEVEL DENSITY AND MEAN RADIATION WIDTHS OF TRANSACTINIDES

G.V. Antsipov, V.A. Kon'shin, V.M. Maslov

Very few experimental data on neutron cross-sections for transactinides are available. In order to calculate neutron cross-sections we need to know the nuclear level density $\rho(U,J)$ and the total radiation widths $\Gamma\gamma(U,J)$. However, we may use experimental data on the low-lying level spectrum for each nucleus separately. The upper limit of the discrete spectrum of levels for transactinides, determined experimentally, usually equals 0.5-1.5 MeV. At higher energies, different level density models are used. Since the values calculated for neutron cross-sections, especially for radiative capture and inelastic scattering, depend on the level density models used and on the parameters of these models, the correctness of the models and the systematics of the corresponding parameters are particularly important.

In this paper, the experimental data were analysed using a superfluid nucleus model taking into account collective modes. A level density parametrization was carried out for deformed axisymmetric nuclei in the mass number range A = 230-250, for which rotational effects on the level density are significant.

Level density model. The level density of deformed transactinide nuclei having axial and mirror symmetry in equilibrium deformations may be represented in the form [1]

$$\tilde{\rho}(U,J)=\frac{\omega(U)}{2\sqrt{2\pi}\sigma_{\parallel}}\sum_{K=-J}^{J}\exp\left[-\frac{J(J+1)}{2\sigma_{\perp}^{2}}-K^{2}\left(\frac{1}{2\sigma_{\parallel}^{2}}-\frac{1}{2\sigma_{\perp}^{2}}\right)\right]. \qquad (1)$$

Here $\sigma_{\perp}$ and $\sigma_{\parallel}$ are spin dependence parameters, linked with the perpendicular ($F_{\perp}$) and parallel ($F_{\parallel}$) moments of inertia of the nucleus; K is the projection of the angular momentum on the axis of symmetry; $\omega(U)$ is the total intrinsic excited state density, which is equal to $\exp S/[(2\pi)^{3/2}\det^{1/2}]$, where S is the entropy, and $\det = 18/\pi^{4}a^{3}t^{5}$

(t being the temperature of the excited nucleus, and a the level density parameter).

As in the adiabatic approximation, it is possible, in computing the rotational degrees of freedom in expression (1) also to take into account the vibrational degrees of freedom [2]:

$$K_{vib}(U) = \exp\left[1{,}7\left(\frac{3m_0A}{4\pi\sigma_{mc}}\right)^{2/3}\left(\frac{C_{mc}}{C}\right)^{2/3}t^{4/3}\right],$$

where σ_{mc} is the surface tension coefficient in the liquid drop model ($4\pi r^2\sigma_{mc}$ = 18 MeV); the ratio C_{mc}/C describes the distinction between the excited nucleus stiffness coefficients and the liquid-drop values (here it is assumed to be equal to unity). Then

$$\rho(U,J) = K_{vib}(U)\tilde{\rho}(U,J).$$

The thermodynamic functions of the nucleus in the superfluid state were determined by the Ignatyuk-Shubin model [3, 4], in which the temperature dependence of the correlation functions is taken into account.

The shell dependence of the level density may be computed, assuming that the level density parameter a is energy-dependent [4]:

$$a = \tilde{a}\left[1 + \frac{f(U-E_{cond})}{U-E_{cond}}\delta W_{exp}\right];$$
$$a_{cr} = \tilde{a}\left[1 + \frac{f(U_{cr}-E_{cond})}{U_{cr}-E_{cond}}\delta W_{exp}\right]. \qquad (2)$$

Here $\tilde{a}$ is the asymptotic value of a; a_{cr} is the value of a at an excitation energy U_{cr}; and $f(U) = 1 - \exp[-\gamma(U - E_{cond})]$, where γ is an empirical parameter.

The expressions shown correspond to an even-even nucleus. Even-odd differences may be taken into account by an appropriate shift in the excitation energy [5]:

$$U^* = U + \begin{cases} \Delta_{ON} & \text{- even-odd nuclei} \\ \Delta_{OZ} & \text{- odd-even nuclei} \\ \Delta_{OZ} + \Delta_{ON} & \text{- odd-even nuclei.} \end{cases}$$

Experimental nuclear mass values and the parameters of the Myers-Swiatecki liquid drop model [6] were used to calculate the shell corrections δW_{exp}. The values of the correlation functions Δ_Z and Δ_N were determined from pairing energies on the basis of data from Ref. [7]. The remaining parameters were taken from Ref. [4]. Note that in those cases where the thermodynamic temperature t for $U = B_n$ is less than t_{cr}, $a_{cr} = a(Bn)$ was assumed for $t \leq t\ (B_n)$, while for $t \geq t\ (B_n)$ dependence (2) was used.

The only parameter in the model described above is the so-called main level density parameter a, which is proportional to the level density near the Fermi energy. This is determined using the value of the density of neutron s-resonances.

If we try to use the model set out above to describe the increasing sums of levels N(E) for those transactinides for which extensive spectroscopic data have been accumulated, we obtain unsatisfactory results (Fig. 1). An acceptable description of N(E) may be obtained by using the Gilbert-Cameron approach [8], according to which the dependence N(E) can be described by a straight line on a semilogarithmic scale, i.e.

$$\rho_1(E) = \frac{d\ N(E)}{dE} = \frac{1}{T} \exp\left(\frac{E - E_0}{T}\right). \qquad (3)$$

Here E_0 and T are parameters of the model, where $T = \left[\frac{d}{dE} \ln \rho_1(E)\right]^{-1}$. An example of how to use expression (3) is shown in Fig. 1. The reason for the sharp change in the slope of N(E) is the omission of levels. In the case of odd-odd nuclei and of nuclei with odd A, a dependence of the type of (3) is not observed. However, it must be remembered that the level density for these nuclei is considerably higher than that for even-even nuclei. Consequently, the number of omitted levels is also much greater, which would appear to explain the acceptable description of the increasing sum of levels N(E) for odd-odd nuclei.

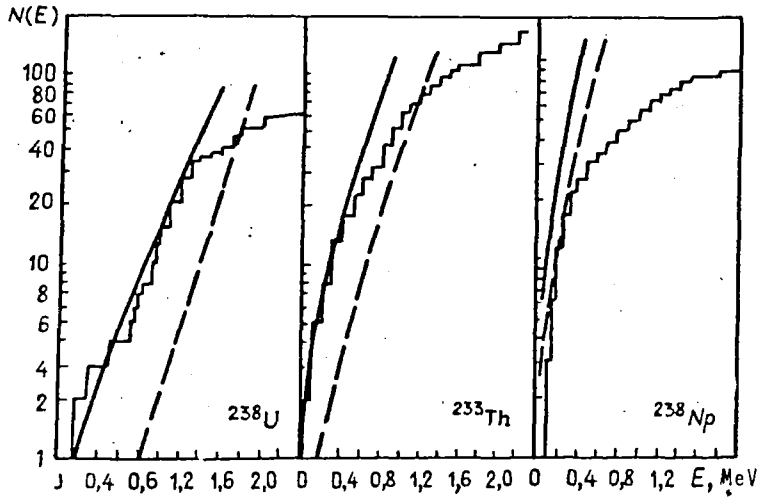

Fig. 1. Dependence N(E) for ^{238}U, ^{233}Th and ^{238}Np. Calculation based on --- superfluid, —— constant-temperature model.

The constant-temperature model is an extremely simple parametrization of the level density. It was used, for example, in Refs [9, 10]; there, however, the neutron resonance density was calculated using the Fermi-gas model, and the transactinides were not considered in Ref. [9].

The selection of parameters for a constant-temperature model should be guided by the following criteria:

(1) An acceptable description of the increasing sum of low-lying levels N(E);

(2) $\rho_1(E_c) = \rho_2(E_c)$ or $E_0 = E_c - T\ln[\rho_2(E_c)\,T]$;

(3) $$\frac{d}{dE}\ln\rho_1(E)\Big|_{E=E_c} = \frac{d}{dE}\ln\rho_2(E)\Big|_{E=E_c} \quad \text{or} \quad \frac{1}{T} = \frac{d}{dE}\ln\rho_2(E)\Big|_{E=E_c};$$

where $\rho_1(E)$ and $\rho_2(E)$ are the level densities in the constant-temperature model and in a superfluid nucleus model taking into account pairing correlations and the contribution of collective modes. In Ref. [10] only the condition of equality of the level density was taken into account, but this condition was very often not satisfied at excitation energies lower than the neutron binding energy. In such cases the exponential dependence was multiplied by a constant selected from the condition for the description $\langle D\rangle_{exp}$. Note that condition (3) takes the form $1/T = \sqrt{a/E_c} - 3/2E_c$ in the Fermi-gas model, while in the case where

rotational degrees of freedom are taken into account in the adiabatic approximation it is $1/T = \sqrt{a/E_c} - 1/E_c$.

Parameterization results. Values of the parameter a and its asymptotic value $\tilde{a}$ were obtained on the basis of experimental data on neutron resonance density from Ref. [11], which are reviewed in Ref. [12]. To calculate the moment of inertia $F_{\|}$, a quasiclassical evaluation of the single-particle angular momentum $\overline{m}^2 = 0.24A^{2/3}$ was used, the quadrupole deformation parameter ϵ being taken to equal 0.24. To describe the attenuation of shell effects, the authors used the value of the parameter $\gamma = 0.064$ obtained in Ref. [4] by minimizing the spread of values of $\tilde{a}$ for nuclei $150 \leq A \leq 245$ with reference to the quasiclassical dependence. It was found that the use of experimental values for neutron and proton pairing energies as correlation functions, while reducing the absolute values of the parameters a and $\tilde{a}$ as compared with the use of the dependence $\Delta_0 = 12/\sqrt{A}$ leads to practically no change in their spread; for this reason, all parameters have been obtained for $\Delta_0 = 12/\sqrt{A}$ below.

Analysis of the constant-temperature model parameters T and E_0 obtained for nuclei with known $\langle D \rangle_{exp}$ and low-lying level spectrum shows that the values of T practically equal $\overline{T} = 0.385$ MeV. In the case of odd nuclei, the fluctuations in $\overline{T}$ are greater, but the mean value of $\overline{T}$ is practically the same as for even-even nuclei. This is evidence that $\overline{T}$ is independent of the parity of nuclei. The extremely low value of $\overline{T}$ for the ^{245}Pu nucleus is due to the unreliable determination of $\langle D \rangle_{exp}$ (from four resonances in the fission cross-section) and the poorly studied spectrum of low-lying states.

The values of the parameter E_0 for even-even nuclei cluster closely around zero, while for odd nuclei $E_0 \approx 0.7$ MeV. From this we may conclude that the quantity E_0 has the meaning of an even-odd shift in excitation energy equal to the value of the correlation function Δ_0 for the ground state. This is confirmed by the clustering of values of $E_0 + \Delta_0$ near

zero for nuclei with a well-studied spectrum (see Fig. 3.) The fluctuations of E_0, as in the case of $\bar{T}$, may be explained by the omission of levels and by errors in determining $\langle D \rangle_{exp}$.

For nuclei with insufficiently studied spectra of low-lying states we can use the average parameters $\bar{T} = 0.385$ MeV and $E_0 = 0$ or $E_0 = -\Delta_0$ for even-even and odd nuclei, respectively. Note that using these average parameters yields a fully satisfactory description of the increasing sums of levels for nuclei, primarily even-even nuclei, the spectrum of which has been studied in some detail, but for which data on $\langle D \rangle_{exp}$ are lacking.

The satisfactory description of the increasing sums of levels for odd-odd nuclei following a superfluid nucleus model taking collective effects into account is a consequence of extensive omission of levels, since the dependence N(E) behaves exactly the same as in the case of odd nuclei, whereas it should increase much more rapidly. We may therefore suppose (by analogy with the odd nuclei) that in this case $E_0 = -2\Delta_0$, and $\bar{T} = 0.385$ MeV.

The systematics of the parameters T and E_0 may be used to calculate the main level density parameter a. Then $\langle D \rangle_{exp}$ can be recovered to serve as a criterion for the validity of the proposed systematics. On the basis of the values of $\bar{T}$ and E_0, it is possible to obtain from the conditions for smooth joining the parameters E_c and a. Since the values of E_c are similar to quantity U_{cr}, and the corrections δW_{exp} are such that the energy dependence a(U) is comparatively weak, the assumption that $a_{cr} = a(E_c)$ does not affect the accuracy of the calculation. The results of calculations in the form of the ratio $\langle D \rangle_{theor}/\langle D \rangle_{exp}$ are shown in Fig. 2. As can be seen, the majority of values obtained falls within the range of $\pm$ 50%. Exceptions are the nuclei ^{238}Np, ^{245}Pu, ^{243}Cm and ^{253}Cf, with $\langle D \rangle_{exp}$ for ^{245}Pu and ^{253}Cf being very unreliable. This difference between the experimental and theoretical values for <D> may be due either to the spread in the available experimental data or to the neglect of certain physical effects in the authors' calculations.

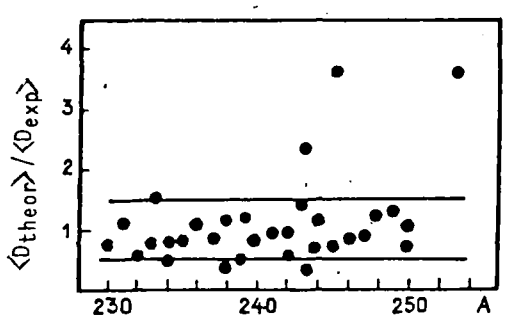

Fig. 2. Ratio of <D> calculated on the basis of average parameters of the constant-temperature model to experimental values.

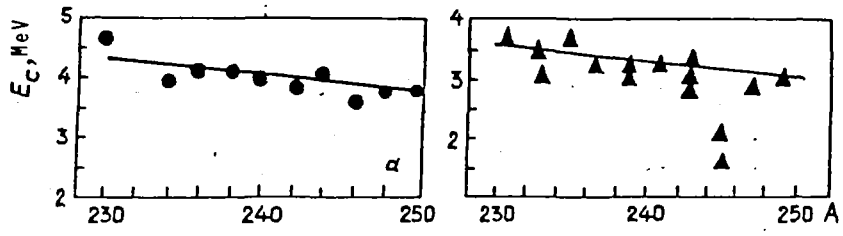

Fig. 3. Comparison of parameters E_c obtained from systematics with those from experiments: a - even-even nuclei, b - odd nuclei.

The fluctuations of the parameters T, E_0, E_c and $a(E_c)$ may be due not only to the omission of levels in the discrete spectrum and to the unreliability of determination of $\langle D \rangle_{exp}$, but also to the representation of the correlation function $\Delta_0 = 12/\sqrt{A}$ used. This dependence significantly exaggerates the neutron pairing energies. However, using the experimental values of the neutron and proton pairing energies $\Delta_{ON} = \Delta_{ONexp}$ and $\Delta_{OZ} = \Delta_{OZexp}$ [7] as correlation functions does not substantially reduce the fluctuation of the parameters; moreover, it is accompanied by a convergence of the values of E_c for even-even and odd nuclei. As a result, even a reduction in the fluctuation of the ratio $\langle D \rangle_{theor}/\langle D \rangle_{exp}$ is not observed.

Let us analyse the parameters E_c and a obtained from the systematics of the parameters T and E_0. Figure 3 gives a comparison of the calculated value of E_c with values obtained from the condition for the description of N(E). There is a striking linear dependence of E_c on the mass number A. Figure 4 compares the ratios of the parameter $a(B_n)$ and its asymptotic value $\tilde{a}$ to the mass number, as calculated from systematics, with those obtained from data on $\langle D \rangle_{exp}$. The dependence of the parameter $a(B_n)$ on the mass number

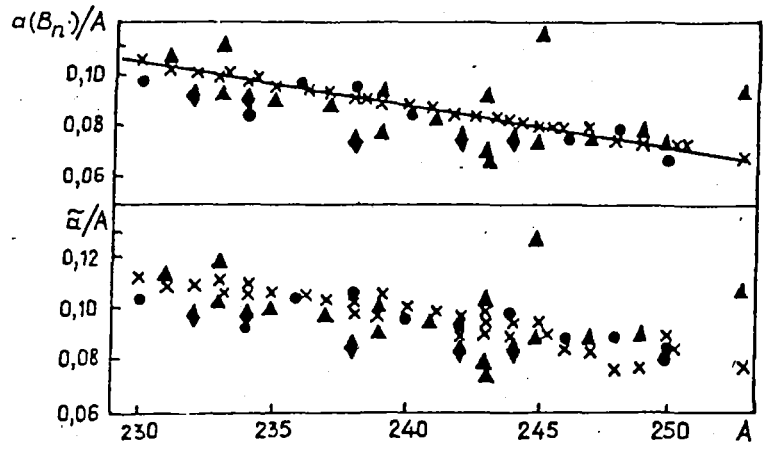

Fig. 4. Comparison of ratios $a(B_n)/A$ and $\tilde{a}/A$ calculated (x) from systematics with those obtained from data on $\langle D \rangle_{exp}$ for: • - even-even, ▲ - odd, ◆ - odd-odd nuclei.

may be represented in the form $a(B_n)/A = -1.619 \times 10^{-3} A + 0.4730$. The parameters of this dependence are appreciably different from the parameters of other authors' systematics.

Let us consider the fluctuations of the parameters of the constant-temperature model due solely to fluctuations in $\langle D \rangle_{exp}$. For this purpose the parameters T and E_c were calculated for E_0 equal to 0, $-\Delta_0$ and $-2\Delta_0$, for even-even, odd and odd-odd nuclei. The values of T obtained for A = 230-280 are close to the value $\bar{T} = 0.388$ MeV. The dense clustering around the parameter $\bar{T} = 0.388$ MeV, except for the nuclides ^{245}Pu and ^{253}Cf, bears witness to the comparative reliability of the data on $\langle D \rangle_{exp}$. Figure 5 gives dependences $E_c(A)$ calculated for $\bar{T} = 0.388$ MeV and E_0 equal to 0, $-\Delta_0$, $-2\Delta_0$ also for nuclei with the corresponding parity in the number of nucleons, as well as data obtained using $\langle D \rangle_{exp}$. It will be seen that they agree closely.

Dependence of the level density on spin and parity. Since the deformation of transactinides is small ($\varepsilon \approx 0.24$), it is possible, for small values of the angular momentum, to write the J-factor describing the spin dependence in the region of spin values under consideration as follows:

$$f(U, J) = \frac{(2J + 1)\exp\left[-J(J + 1)/2\sigma_\perp^2\right]}{2\sigma_\perp^2}. \qquad (4)$$

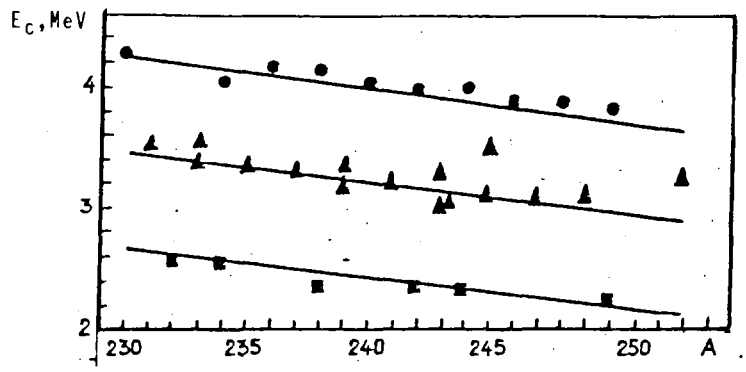

Fig. 5. Comparison of E_c values obtained from $\langle D \rangle_{exp}$ data for E_o equal to $0, -\Delta_0$ and $-2\Delta_0$ for even-even (•), odd (▲) and odd-odd (■) nuclei with values calculated from systematics.

Taking into account collective degrees of freedom does not change the qualitative law of distribution by angular momentum. Let us look at the spin distribution of low-lying levels. Under the assumption of law (4), the method of maximum probability leads us to the following evaluation:

$$\sigma^2_{\perp exp} = 1/2 N \sum_i J_i(J_i+1), \qquad (5)$$

where N is the number of levels identified by their spin. Even though the evaluation in expression (5) is weakly sensitive to omission of levels, only data from the energy region where such omission was comparatively slight were used in determining the value of $\sigma^2_{\perp exp}$. This was determined by describing the growing sum of levels in terms of the constant-temperature model. Figure 6 gives the values of $\sigma^2_{\perp exp}$ obtained for 41 nuclei. Parametrization by the least squares method gives the following dependence of $\sigma^2_{\perp exp}$ on the mass number:

$$\sigma^2_{\perp exp} = 0{,}15624A - 26{,}76. \qquad (6)$$

The value of $\sigma^2_{\perp exp}$ also permits an acceptable description of N(E,J) for ^{235}U (Fig. 7). In practice the same description is observed also for other nuclei with a sufficiently well-studied spectrum.

In describing the energy dependence $\sigma^2_{\perp}(U)$, recourse may be had to the procedure proposed in Ref. [9], where $\sigma^2_{\perp} = \sigma^2_{\perp exp}$ up to the limit of reliable identification of levels E_{lim}, while beyond E_{lim} up to the point E_c at which the superfluid nucleus and constant-temperature models

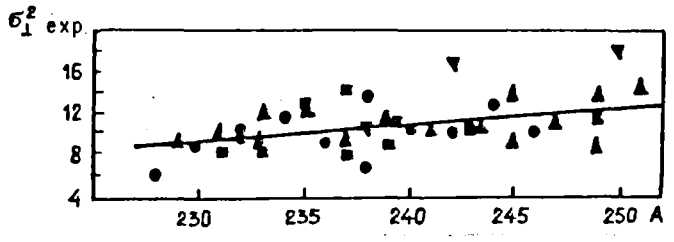

Fig. 6. Dependence of $\sigma^2_{\perp exp}$ on the mass number A:
● - even-even, ▲ - even-odd, ■ - odd-even,
▼ - odd-odd nuclei.

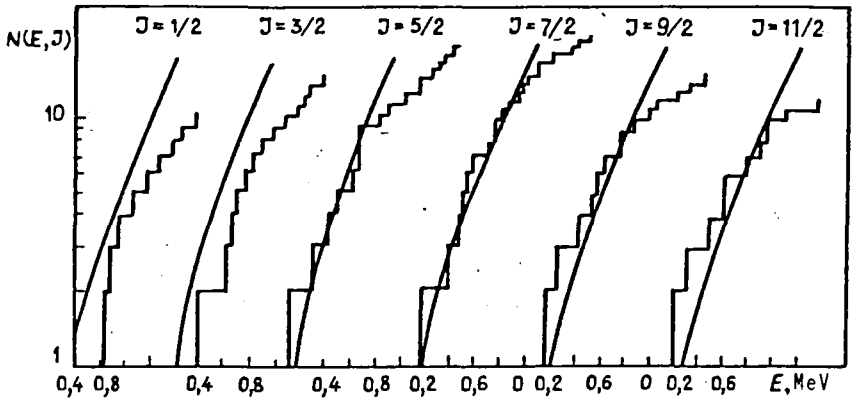

Fig. 7. Description of N(E,J) for ^{235}U in the constant-temperature model.

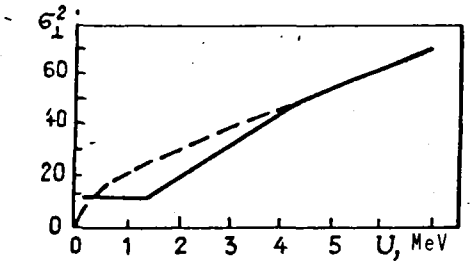

Fig. 8. Dependence $^2(U)$ for ^{234}U according to superfluid nucleus model (---) and as recommended.

join the quantity $\sigma^2_{\perp}$ is determined by linear interpolation between $\sigma^2_{\perp exp}$ and $\sigma^2_{\perp}(E_c)$ calculated using the superfluid nucleus model. For nuclei whose discrete spectrum has been identified insufficiently completely to allow evaluation of quantity $\sigma^2_{\perp exp}$, it is possible to use the dependence (6) and the values E_{lim} = 1.2 MeV for even-even nuclei, E_{lim} = 0.6 MeV for odd nuclei, and E_{lim} = 0.3 MeV for odd-odd nuclei these being averages for the corresponding classes of nuclei. Figure 8 gives a comparison of the characteristic dependence of the recommended and parameter $\sigma^2_{\perp}$ for ^{234}U, and that calculated from the superfluid model.

Finally, let us consider the dependence of the level density on parity. As a rule, the models make use of ideas concerning the probable

parity distribution of the levels. Analysis of the characteristics of the discrete spectrum of 51 nuclei from thorium to californium has shown that for 69% the relationship $\rho_+ = \rho_-$ holds within limits of ± 50%. In view of the inadequate reliability with which the parity of levels is determined and of the small amount of statistics, such agreement seems sufficient to consider the assumption $\rho_+ = \rho_-$ as not contradicting the available data for low excitation energies in heavy deformed nuclei.

Data on the level density parameters for the transactinides (obtained using $\Delta_0 = 12/\sqrt{A}$) in the range ^{225}Th–^{254}Cf are given in the Table.

Data on level density parameters for transactinides

Compound nucleus	I^π	B_n, MeV	$\langle D\rangle_{exp}$, eV	$a(B_n)$, MeV^{-1}	$\tilde{a}$, MeV^{-1}	$\langle D\rangle_{I+1/2}$, eV	$\langle D\rangle_{I-1/2}$, eV
^{225}Th	0+	5,760	—	24,550	24,955	2,725	—
^{226}Th	(3/2+)	7,181	—	24,250	25,232	0,309	0,498
^{227}Th	0+	5,456	—	23,950	24,935	5,640	—
^{228}Th	(3/2$^+$)	7,128	—	23,702	25,052	0,365	0,589
^{229}Th	0$^+$	5,239	—	23,400	24,614	9,598	—
^{230}Th	5/2$^+$	6,790	0,4[illegible]	22,349	23,669	0,701	0,932
^{231}Th	0$^+$	5,128	9,8±1,6	24,614	26,080	9,80	—
^{232}Th	5/2$^{(+)}$	6,434	—	22,550	23,897	1,346	1,794
^{233}Th	0$^+$	4,787	16,6±0,9	26,039	27,408	16,60	—
^{234}Th	(1/2$^+$)	6,179	—	21,950	23,097	5,326	15,720
^{229}Th	(3$^+$)	7,045	—	23,434	24,703	0,064	0,081
^{230}Pa	(5/2)	5,786	—	23,125	24,701	0,186	0,248
^{231}Pa	(2$^-$)	6,818	—	22,838	23,226	0,142	0,206
^{232}Pa	(3/2$^-$)	5,560	0,37	21,259	22,902	0,593	0,967
^{233}Pa	(2$^-$)	6,520	—	22,287	23,807	0,277	0,400
^{234}Pa	3/2$^-$	5,197	0,69	21,432	23,049	1,118	1,802
^{235}Pa	4$^{(+)}$	6,122	—	21,673	22,902	0,456	0,534
^{236}Pa	(3/2$^-$)	4,840	—	21,358	22,558	2,243	3,627
^{237}Pa	(1$^-$)	5,930	—	21,117	21,975	1,563	3,059
^{238}Pa	(1/2$^+$)	4,480	—	20,801	21,477	8,220	24,284
^{229}U	0$^+$	6,091	—	23,400	24,744	1,509	—
^{230}U	(3/2$^+$)	7,662	—	23,143	24,870	0,141	0,227
^{231}U	0$^+$	5,898	—	22,800	24,710	2,438	—
^{232}U	(5/2)	7,264	—	22,590	24,665	0,248	0,332
^{233}U	0$^+$	5,744	4,1	21,655	23,916	4,10	—
^{234}U	5/2$^+$	6,841	0,61±0,07	19,933	21,986	1,067	1,423
^{235}U	0$^+$	5,305	10,6±0,5	21,251	23,500	10,60	—
^{236}U	7/2$^-$	6,546	0,438±0,038	22,614	24,863	0,801	0,967
^{237}U	0$^+$	5,125	16,2±0,8	20,837	23,023	16,20	—
^{238}U	1/2$^+$	6,143	3,5±0,8	22,707	24,700	4,686	13,831
^{239}U	0$^+$	4,804	20,8±1,0	23,611	25,628	20,80	—
^{240}U	5/2$^+$	5,933	—	20,209	21,692	5,115	6,847
^{233}Np	(4$^+$)	7,350	—	22,356	24,453	0,039	0,046
^{234}Np	(5/2$^+$)	6,130	—	22,054	24,054	0,122	0,164
^{235}Np	(0$^+$)	6,991	—	21,762	24,196	0,369	—
^{236}Np	5/2$^+$	5,690	—	21,439	24,125	0,318	0,427
^{237}Np	(6$^-$)	6,621	—	21,196	23,535	0,162	0,173
^{238}Np	5/2$^+$	5,480	0,740±0,061	17,935	20,163	1,293	1,730
^{239}Np	2$^+$	6,226	—	20,575	22,662	0,690	1,001

Compound nucleus	I^{π}	B_n, MeV	<D> exp, eV	$a(B_n)$, MeV^{-1}	$\tilde{a}$, MeV^{-1}	$<D>_{I+1/2}$, eV	$<D>_{I+1/2}$, eV
^{240}Np	$5/2^+$	5,164	—	20,268	22,525	1,114	1,496
^{241}Np	(5^+)	5,970	—	19,959	21,690	0,773	0,861
^{233}Pu	0^+	6,370	—	22,290	24,327	1,039	—
^{234}Pu	—	7,768	—	—	—	—	—
^{235}Pu	0^+	6,252	—	21,712	24,418	1,496	—
^{236}Pu	$(5/2^+)$	7,354	—	21,500	24,250	0,257	0,345
^{237}Pu	0^+	5,860	—	21,152	24,119	3,446	—
^{238}Pu	$7/2^-$	6,998	—	20,891	23,730	0,470	0,572
^{239}Pu	0^+	5,655	9,2±0,7	18,743	21,560	9,200	—
^{240}Pu	$1/2^+$	6,534	2,15±0,04	20,895	23,669	2,877	8,508
^{241}Pu	0^+	5,241	13,0±0,3	20,428	23,187	13,00	—
^{242}Pu	5/2	6,301	1,20±0,07	20,741	23,173	2,095	2,809
^{243}Pu	0^+	5,037	13,5±0,3	22,571	25,283	13,500	—
^{244}Pu	$(7/2^+)$	6,018	—	—	—	—	—
^{245}Pu	0^+	4,720	11,4±4,0	28,393	31,071	11,400	—
^{246}Pu	$(9/2^-)$	5,942	—	18,394	20,044	4,989	5,704
^{239}Am	1^+	7,100	—	20,699	23,837	0,201	0,395
^{240}Am	$(5/2^-)$	5,900	—	20,386	23,885	0,279	0,376
^{241}Am	(3^-)	6,582	—	20,060	23,042	0,323	0,412
^{242}Am	$5/2^-$	5,529	0,58±0,04	18,310	21,156	1,013	1,357
^{243}Am	1^-	6,376	—	19,437	21,966	1,012	1,987
$^{243}Am^*$	5^-	6,425	0,45	16,982	19,173	0,849	0,957
^{244}Am	$5/2^-$	5,364	0,68±0,06	18,661	21,313	1,188	1,591
^{245}Am	(6^-)	6,046	—	18,806	20,904	0,813	0,875
^{246}Am	$(5/2^+)$	5,055	—	18,452	20,630	2,134	2,678
^{239}Cm	0^+	6,400	—	20,643	24,116	1,387	—
^{240}Cm	(7/2)	7,400	—	20,377	23,799	0,251	0,306
^{241}Cm	0^+	6,071	—	20,039	23,740	2,943	—
^{242}Cm	$1/2^+$	6,969	—	19,749	23,055	1,691	5,008
^{243}Cm	0^+	5,701	17,6±3,3	16,213	19,016	17,600	—
^{244}Cm	$5/2^+$	6,799	0,50±0,20	20,339	23,657	0,874	1,169
^{245}Cm	0^+	5,519	11,8±1,2	18,488	21,705	11,800	—
^{246}Cm	$7/2^+$	6,451	1,14±0,14	18,726	21,635	2,083	2,519
^{247}Cm	0^+	5,157	21,3±5,3	18,716	21,665	21,300	—
^{248}Cm	$9/2^-$	6,210	1,2	19,536	22,251	2,262	2,554
^{249}Cm	0^+	4,713	40,0±5,0	19,687	22,174	40,000	—
^{250}Cm	$(1/2^+)$	5,833	—	17,060	18,667	25,222	74,729
^{244}Bk	$(3/2^-)$	6,110	—	19,258	22,761	0,360	0,586
^{245}Bk	(4^-)	6,990	—	18,959	22,172	0,183	0,217
^{246}Bk	$(3/2^-)$	5,900	—	18,591	21,869	0,638	1,039
^{247}Bk	(2^-)	6,600	—	18,235	21,353	0,675	0,983
^{248}Bk	$(3/2^-)$	5,280	—	17,907	21,294	2,229	3,628
^{249}Bk	(6^+)	6,500	—	17,565	20,278	0,526	0,571
^{250}Bk	$7/2^+$	4,969	1,1	18,434	21,150	2,008	2,433
^{251}Bk	(2^-)	5,800	—	16,710	18,403	4,148	6,048
^{245}Cf	0^+	6,145	—	18,896	22,568	3,407	—
^{246}Cf	—	7,354	—	—	—	—	—
^{247}Cf	0^+	6,020	—	18,217	22,039	5,152	—
^{248}Cf	$(7/2^+)$	7,000	—	17,946	21,609	0,948	1,163
^{249}Cf	0^+	5,594	—	17,537	21,247	12,976	—
^{250}Cf	$9/2^-$	6,618	1,07±0,14	17,252	20,571	2,010	2,288
^{251}Cf	0^+	5,114	—	16,729	19,750	37,762	—
^{252}Cf	$1/2^+$	6,165	—	16,334	18,725	17,120	50,733
^{253}Cf	0^+	4,792	16	24,082	27,127	16,000	—
^{254}Cf	$(7/2^+)$	6,029	—	15,343	16,865	10,774	13,245

Radiation widths. Let us consider the application of the model $\rho(U,J)$ described above to the calculation of the mean radiation widths $\langle\Gamma_\gamma\rangle$ of neutron resonances. The theoretical analysis of $\langle\Gamma_\gamma\rangle$ will be based on the following assumptions:

(1) The photoabsorption cross-section $\sigma_\gamma(\varepsilon_\gamma)$ does not depend on the excitation energy of the nucleus (Axel-Brink hypothesis);

(2) The main contribution to the width $\langle\Gamma_\gamma\rangle$ is from El-transitions. In that case the mean total radiation width of a neutron resonance with spin J at an excitation energy U can be represented in the form

$$\langle\Gamma_\gamma(U,J)\rangle = \frac{1}{3}\,\frac{1}{(\pi\hbar c)^2}\int_0^U \varepsilon_\gamma^2\,\sigma_\gamma(\varepsilon_\gamma)\sum_{I=|J-1|}^{J+1}\frac{\rho(U-\varepsilon_\gamma, I)}{\rho(U,J)}\,d\varepsilon_\gamma .$$

At excitation energies of the same order as the neutron binding energy it is necessary to know the photoabsorption cross-section in the range $\varepsilon_\gamma \leq B_n$. Usually this is determined from the parametrization of the giant dipole resonance (GDR) obtained in the region of comparatively high excitation energies ($\varepsilon_\gamma > 7$ MeV). Direct data on the cross-section $\sigma\gamma(\varepsilon\gamma)$ in the low-energy region are lacking. References [13, 14] contain attempts at a theoretical analysis of the El-photoabsorption cross-section in a semi-microscopic approach to the description of the GDR. It was found in Ref. [14] that the quantity $\sigma_\gamma(\varepsilon_\gamma)$ was substantially smaller than the values obtained by extrapolation of the GDR in the region of the low-energy "tail":

$$\sigma_\gamma(\varepsilon_\gamma) = 4\pi\,\frac{e^2\hbar}{Mc}\,\frac{NZ}{A}\,\frac{\varepsilon_\gamma^2\,\Gamma_\sigma}{(\varepsilon_\gamma^2 - E_\sigma^2)^2 + \varepsilon_\gamma^2\,\Gamma_\sigma^2},$$

where $\Gamma_\sigma \approx 3$ MeV; $E_\sigma \approx 85/\sqrt[3]{A}$. Performing such calculations by the methods of the theory of finite Fermi systems is extremely time-consuming, and the accuracy achieved in doing so is not acceptable for the calculation of radiative capture cross-sections $\sigma_\gamma(E)$.

Reference [15] describes measurements of the photoabsorption cross-section for ^{238}U for $\varepsilon_\gamma \geq 6$ MeV. The authors of Ref. [16] parametrized the cross-section $\sigma_\gamma(\varepsilon_\gamma)$ in the region of the low-energy "tail" for transactinides taking into account the splitting of the GDR:

$$\sigma_\gamma(\varepsilon_\gamma) = \sum_{i=1,2} \sigma_i \frac{\varepsilon_\gamma^2 \Gamma_{\sigma_i}^2}{(\varepsilon_\gamma^2 - E_{\sigma_i}^2)^2 + \varepsilon_\gamma^2 \Gamma_{\sigma_i}^2}. \quad (7)$$

The parameters obtained, $\sigma_1 = 250$ mb, $E_{\sigma_1} = 10.5$ MeV, $\Gamma_{\sigma_1} = 2.5$ MeV, $\sigma_2 = 300$ mb, $E_{\sigma_2} = 14$ MeV, $\Gamma_{\sigma_2} = 4.5$ MeV, differ from the parameters which, in describing the GDR, exaggerate the value of $\sigma_\gamma(\varepsilon_\gamma)$ in the low-energy region.

The results of calculations, in the form of the ratio $\langle\Gamma_\gamma\rangle_{exp}/\langle\Gamma_\gamma\rangle_{theor}$, of widths averaged with respect to the spin distribution of the compound nucleus using expression (7) are given in Fig. 9. The proposed system for calculating $\langle\Gamma_\gamma(U,J)\rangle$ provides a description of the observed total radiation widths within the limits of

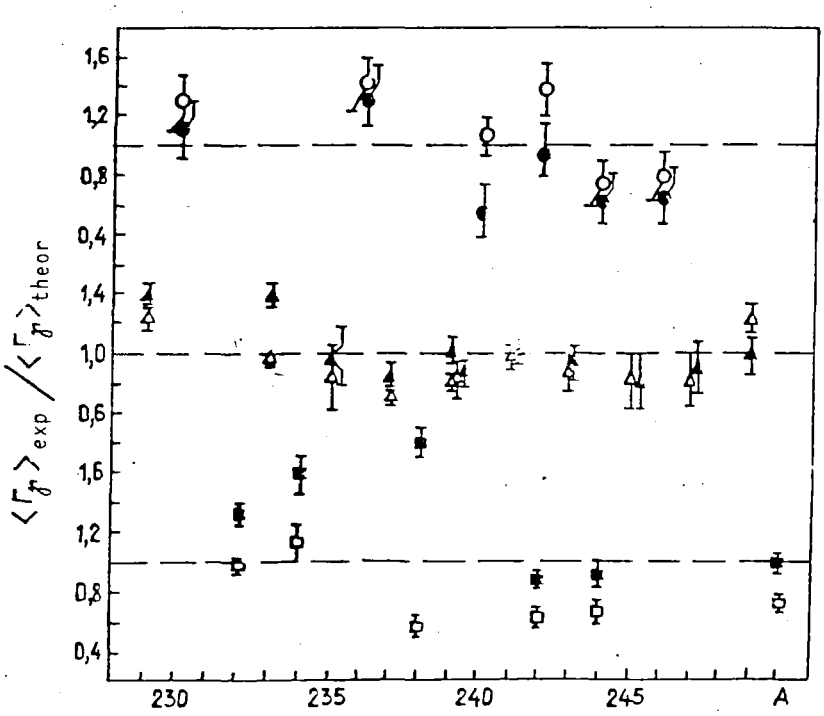

Fig. 9. Dependence of $\langle\Gamma_\gamma\rangle_{exp}/\langle\Gamma_\gamma\rangle_{theor}$ on the mass number A. For the superfluid nucleus model: even-even (•), odd (▲), odd-odd (■); 0, Δ, □ - the same for the constant-temperature model.

experimental error for half the nuclei on which there are data; in the general case the accuracy of the calculations is not worse than about 30%. Note that for even-even compound nuclei, the calculation results are observed systematically to exceed the experimental data by approximately 30%, while in the case of odd-odd nuclei the relationship is reversed, the difference also amounting to approximately 30%.

Figure 9 shows that the calculation results for the general case depend on the paramtrization of the level density at low excitation energies, although in different ways for even-even and odd-odd compound nuclei. This is a consequence of the parametrization of the spin dependence $\rho(U,J)$ and the comparatively low values of the spins of N-odd compound nuclei.

From the aforesaid it is possible to draw the following conclusions:

1. On the basis of the results of contemporary experiments, the level density parameters $\tilde{a}$ and a were obtained, in a superfluid nucleus model taking into account collective degrees of freedom, for transactinides;
2. The parameters of a constant-temperature model permitting recovery of the value $\langle D \rangle_{exp}$ with an error of no worse than $\pm$ 50% were obtained;
3. It was shown that in order to account for even-odd differences in the level density it is sufficient to introduce in the constant-temperature model a shift in the excitation energy equal to $-\Delta_0$ for odd and $-2\Delta_o$ for odd-odd nuclei;
4. From the parameter systematics for the constant-temperature model the dependence of the level density parameter a on the mass number A was obtained;
5. The results of the systematics yield an evaluation of the reliability of experimental data on $\langle D_{exp} \rangle$. Thus, the experimental values for ^{245}Pu and ^{253}Cf are unreliable, most often understating by a factor of about 2;

6. A systematic evaluation of $\sigma^2_{\perp exp}$ yielded its dependence on the mass number A;

7. The legitimacy of applying the same spin distribution law in the regions of both high (around B_n) and low excitations for a suitably selected parameter $\sigma^2_\perp$ was demonstrated;

8. It was shown that the assumption of independence of the level density on parity at low excitation energies is confirmed by an analysis of the characteristics of the discrete-spectrum levels of transactinides;

9. The quality of the parametrization of the level density was demonstrated using as an example a calculation of $\langle \Gamma_\gamma \rangle$ employing the parametrization of the low-energy "tail" of the GDR. The results of the description proved no worse than the proposed empirical and semi-empirical systematics.

EVALUATION OF TOTAL INTERACTION CROSS-SECTIONS FOR NUCLEI WITH MASS NUMBER 3

A.G. Zvenigorodskij, B.Ya. Guzhovskij, S.N. Abramovich,
V.A. Zherebtsov, O.A. Pelipenko.

Work in the field of thermonuclear fusion and astrophysical calculation requires increasingly accurate evaluations of the reaction cross-sections for light nuclei over a wide energy range. This paper examines aspects of evaluating cross-sections for the reactions $^{3}H(t,2n)^{4}He$, $^{3}He(^{3}He,2p)^{4}He$, $^{3}He(t,x)n$ and $^{3}He(t,d)^{4}He$. Knowing accurate values of the cross-sections for the first reaction is important for deuterium/tritium plasma diagnosis [1-3]. The importance of the $^{3}He(^{3}He,2p)^{4}He$ reaction as the last in the proton-proton chain is pointed out in Ref. [4], which also gives a review of the experimental data and an evaluation of the S-factor. The total neutron yield from the $^{3}He(t,x)n$ reaction is investigated in Ref. [5].

Despite the extensive literature on the above reactions, the evaluated data have to be constantly updated. This is necessary owing to the appearance of new experimental work which significantly supplements the older evaluations and as a result of the search for more convenient forms (for use on computers) of presentation of the evaluated data.

The evaluation of the total cross-section for the $^{3}He(t,2n)^{4}He$ reaction is based on the references listed in Table 1.

As can be seen from Fig. 1, there is a significant spread in the values for the cross-sections given by various authors, in particular between the

Table 1. References used to evaluate the cross-section for the $^{3}He(t,2n)^{4}$ reaction.

Energy range, MeV	Type of data	Reference
0,06—1,01	$\sigma_t(E)$, $\sigma(90^{o}, E)$	[6]
0,04—2,4	$\sigma_t(E)$	[7]
1,8	σ_t	[8]
0,03—0,1	$\sigma(0^{o}, E)$, $\sigma_t(E)$	[9]
0,04—0,2	$\sigma(0^{o}, E)$	[10]

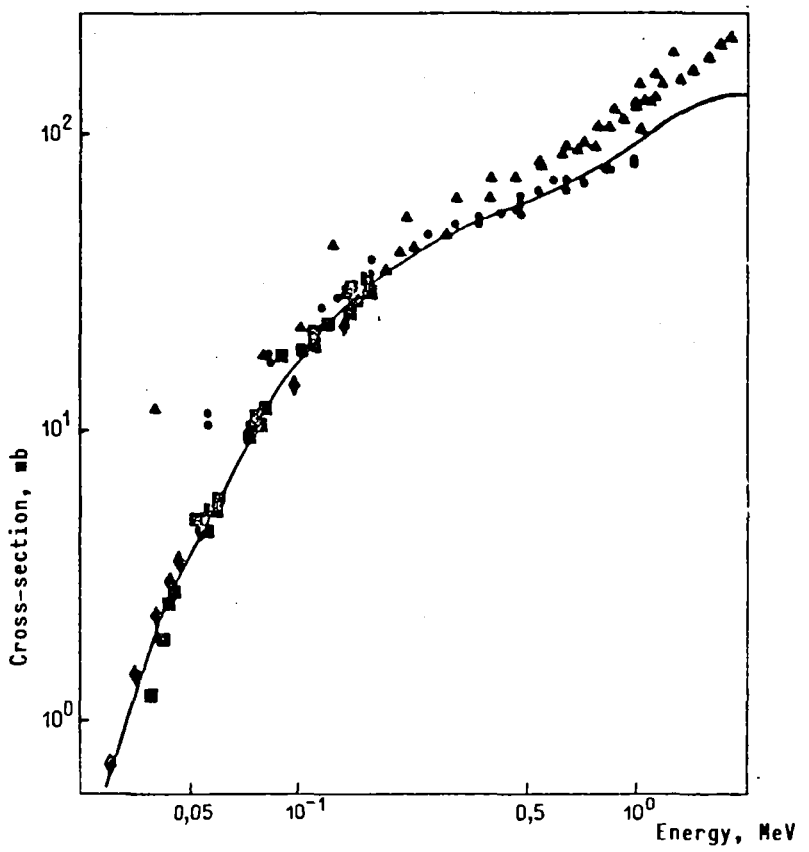

Fig. 1. Energy dependence of the total cross-section for the $^3He(t,2n)^4He$ reaction. Data from the following references: ■ - [10]; ◆ - [9]; ▲ - [7]; ● - [6].

values given in Ref. [7] and those in Refs [6, 9, 10]. At the same time, it should be noted that the previously accepted evaluation of the cross-section for this reaction [11] was based on the results of Ref. [7]. Subsequent R-matrix analysis of the data on the ^6He system [12] gave a better prediction for the behaviour of the cross-section for the $^3H(t,2n)^4He$ reaction which generally agreed with the results of Refs [6, 9, 10].

In finding the evaluated curve, the authors of the present work divided the whole energy range of the data into two regions: the first up to an interaction energy $E_{cm} < 0.025$ MeV (in the centre-of-mass system), and the second from $E_{cm} > 0.025$ MeV. In the lower energy region, the evaluated curve was sought in the form of a Gamow function:

$$\sigma_t(E) = [S(E)/E]\exp(-\alpha/\sqrt{E}). \quad (1)$$

In the general case, the S-function is dependent on the energy and is represented by the expansion:

$$S(E) = S_0 + S'_{(0)}E + 1/2\ S''_{(0)}E^2.$$

Here the coefficient α is given by the theoretical expression $\alpha/\sqrt{E}_{cm} = 2\pi\ \eta$, where η is the Coulomb parameter.

In the case of the (T + T)-interaction, $\alpha = 1.2151\ MeV^{1/2}$. The S-factor was taken from Ref. [9], where it was found using the assumption of linear dependence on energy: $S(E) = S_{(0)} + S'_{(0)}E$, where $S_{(0)} = 105$ mb MeV and $S'_{(0)} = 880$ mb.

At interaction energies $E_{cm} > 0.025$ MeV the evaluated curve was sought using a spline approximation. In doing so, the equality of the logarithmic derivatives at the boundary ($E_{cm} = 0.025$ MeV) of the two regions selected by the authors was used to ensure smoothness and continuity of the transition from one representation of the evaluated curve to the other.

Table 2 shows the set of cubic spline coefficients used to calculate the values of the cross-sections in the region where the evaluation was carried out by means of a spline approximation. The total cross-section for the reaction can be obtained with this set of coefficients using the formula:

$$\sigma_t(E) = \exp\{A_0^{(i)} + A_1^{(i)}\ln(E/E_i) + A_2^{(i)}[\ln(E/E_i)]^2 + A_3^{(i)}[\ln(E/E_i)]^3\}\ , \qquad (2)$$

where E_i is the energy of the i-th node of a spline curve, satisfying the condition $E_i < E < E_{i+1}$. The coefficients $A_0^{(i)}$, $A_1^{(i)}$, $A_2^{(i)}$, $A_3^{(i)}$ correspond to the i-th node in Table 2.

As was shown above, the reaction $^3He(^3He,2p)^4He$ is one of the branches of the proton-proton chain, for which reason its cross-section is of great interest for astrophysical applications. The most recent review of data on this reaction dates back to 1967 [4]. Since then, a number of papers have appeared (Table 3) which add substantially to the evaluation made in Ref. [4].

Table 2. Coefficients of spline curves describing the estimated values of the total cross-section for the $^3He(t,2n)^4He$ reaction (energy in the centre-of-mass system).

Number of spline node	Energy of node, MeV	A_0, mb	A_1, mb	A_2, mb	A_3, mb
1	0,025	1,1504	2,7904	−0,952	0,1204
2	0,0665	3,0807	1,2750	−0,599	0,1421
3	0,1765	3,8873	0,5116	−0,182	0,2003
4	0,469	4,4002	0,7293	0,4051	−0,629
5	1,246	—	—	—	—

Table 3. References used to evaluate the total cross-section for the $^3He(^3He,2p)^4He$ reaction.

Energy range, MeV	Type of data	Reference
0,4—1,4	$\sigma_t(E)$	[13]
0,31—5,9	S(E)	[4]
0,059—2,2	$\sigma_t(E)$, S(E)	[14]
3,9—9,1	$\sigma(\theta)$	[15]
13,6	$\sigma(\theta)$	[16]

It is characteristic of the three-body reaction $^3He(^3He,2p)^4He$ that as the interaction energy increases, the quasi-two-body channel of the $^3He(^3He,p)^5Li$ reaction begins to predominate increasingly in the proton spectrum. In this work, the authors did not separate these two channels. Therefore the evaluation refers to the total cross-section for proton formation in the (^3He + ^3He) interaction. The evaluated excitation function curve for the total cross-section for the $^3He(^3He,2p)^4He$ reaction was found in the following way. On the basis of the experimental data in Ref. [14], fitting was performed by the least-squares method for $E_{cm} < 0.15$ MeV in accordance with formula (1), the S-factor being approximated by a quadratic polynomial.

The following results were obtained (in the centre-of-mass system):

$$S_{(0)} = 5307 \pm 560 \text{ MeV}\cdot\text{mb}$$

$$S'_{(0)} = -2150 \pm 760 \text{ mb}$$

$$1/2\ S''_{(0)} = 793 \pm 510 \text{ mb/MeV}, \quad \alpha = -4.8604 \text{ MeV}^{1/2}.$$

Since the Coulomb barrier in the $^3He + ^3He$ channel is equal to about 1 MeV, it is appropriate to use the cross-section description based on the quasi-classical formula (1) for energies significantly lower than 1 MeV. Hence, for energies higher than 0.15 MeV, the evaluation of the total cross-section for the $^3He(^3He,2p)^4He$ reaction was performed by the spline method for the condition of continuity and smoothness of the approximating function at the point $E_{cm} = 0.15$ MeV.

Figure 2 gives the experimental data used for the evaluation and the evaluated approximating curve. In the authors' opinion, reasonably reliable

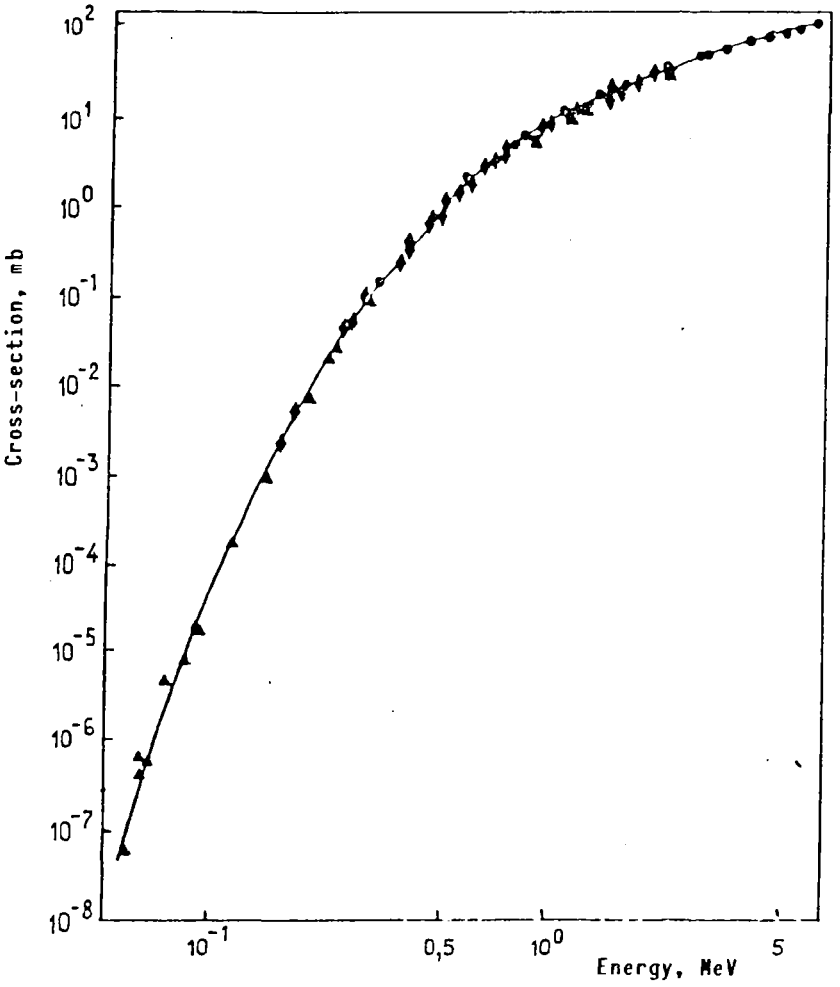

Fig. 2. Energy dependence of the total cross-section for the $^3He(^3He,2p)^4He$ reaction. Data from the following references: ■ - [13]; ◆, ▲ - [14]; ● - [4].

data are available only for energies E_{cm} < 3 MeV, which is why the spline curve was determined only for this value. At higher energies, using data from Refs [15, 16], the growth of the proton formation cross-section for the (^{3}He + ^{3}He) interaction stops (levels off).

The total cross-section for the ^{3}He(^{3}He,2p)^{4}He reaction for energies E_{cm} > 0.15 MeV can be calculated from formula (3) if the spline coefficients from Table 4 are used.

Table 4. Coefficients of spline curves describing the estimated values of the total cross-section for the ^{3}He(^{3}He,2p)^{4}He reaction (energy in the centre-of-mass system).

Number of spline node	Energy of node, MeV	A_0, mb	A_1, mb	A_2, mb	A_3, mb
1	0,15	0,12	0,005	2,4092	3,1468
2	2,8	99,42	0,0	0,0	0,0
3	7,0	—	—	—	—

$$\sigma_t(E) = A_0^{(i)} + A_1^{(i)}\ln(E/E_i) + A_2^{(i)}[\ln(E/E_i)]^2 + A_3^{(i)}[\ln(E/E_i)]^3, \qquad (3)$$

where E_i is the energy of the i-th node of the spline curve, satisfying the condition $E_i < E < E_{i+1}$.

The total cross-section for the cumulative neutron yield from the ^{3}He(t,x)n reaction was evaluated in Ref. [5] for the energy range E_{lab} = 0.25-1.76 MeV. In experimental work [17, 18] appearing after this evaluation, only the cross-section for neutron formation in the channel ^{3}He(t,n)^{5}Li channel was determined; thus it was not possible to determine the total neutron yield with sufficient accuracy and thereby to complete the results of the evaluation in Ref. [5].

In order to make it easier to use the results of the evaluation in Ref. [5], a spline description was made of the estimated values proposed in Ref. [5] for the total cross-section of the cumulative neutron yield in the (^{3}He + T) interaction. The results of the spline approximation are given in Table 5 and Fig. 3.

Table 5. Coefficients of a spline curve for describing the cumulative neutron yield from the (^{3}He + T) interaction (energy in the laboratory co-ordinate system).

Number of spline node	Energy of node, MeV	A_0, mb	A_1, mb	A_2, mb	A_3, mb
1	0,046	−4,483	6,5766	−1,258	−0,199
2	0,114	0,3132	3,7904	−1,801	0,479
3	0,284	2,6335	1,7016	−0,492	−0,0005
4	0,700	3,7744	0,8033	−0,494	−0,068
5	1,758	—	—	—	—

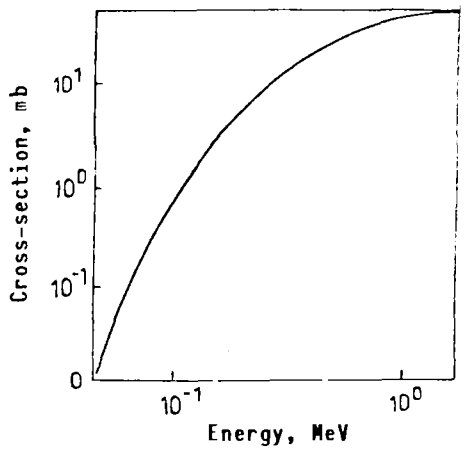

Fig. 3. Energy dependence of the total cross-section for the cumulative neutron yield from the ^{3}He(t,x)n reaction.

The total cross-section for the cumulative neutron yield for the (^{3}He + T) interaction can be found from formula (2).

The cross-section for the ^{3}He(t,d)^{4}He reaction, which is important for astrophysical applications, was studied in Refs [19-21]. In order to use the data from Ref. [19] (which gives absolute values only for the differential cross-sections at angles of 10° and 90°), the angular distributions given in that paper were normalized, and integrals were obtained from them which were then used to determine the Gamow function parameters. These parameters proved to be close to the values given in Ref. [22] [S_0 = 450 mb·MeV, α = 3.44 MeV$^{1/2}$ (in the laboratory co-ordinate system)]. By analysing a comparatively small amount of experimental data using the spline method, we found the following methodological characteristic of the calculation: with such a small number of experimental points there is a very strong dependence of the shape of the evaluated curve on the boundary conditions. Also, it was not possible to get rid of the excess "flexibility" of the spline curve without abandoning the

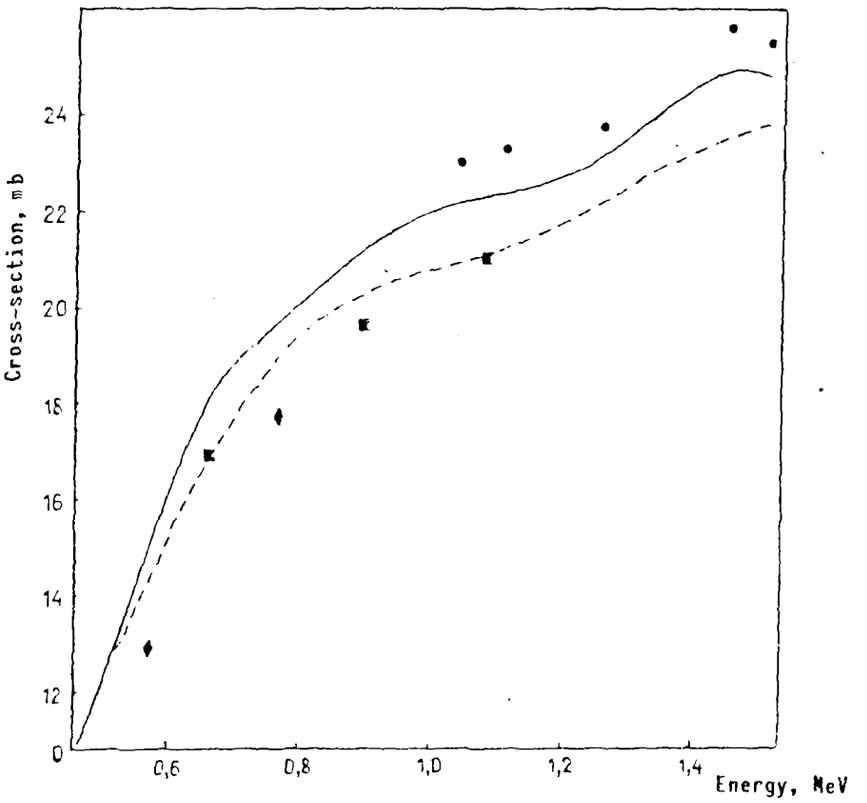

Fig. 4. Energy dependence of the total cross-section for the $^{3}He(t,d)^{4}He$ reaction. Data from the following references: ◆ - [19]; ■ - [21]; ● - [20]. Calculation --- - with continuity of the second derivative at the spline-curve nodes; —— - without limitations on the behaviour of the second derivative at the spline-curve nodes.

Table 6. Coefficients of a spline curve describing the estimated value of the total cross-section for the $^{3}He(t,d)^{4}He$ reaction (energy in the laboratory co-ordinate system).

Number of spline node	Energy of node, MeV	A_0, mb	A_1, mb	A_2, mb	A_3, mb
1	0,460	10,8	29,59	122,1	−440,2
2	0,700	18,85	12,14	6,85	−42,8
3	0,974	21,81	6,27	−28,3	76,9
4	1,247	22,98	8,05	34,83	−151,7
5	1,521	—	—	—	—

condition of continuity of the second derivative at all nodes. Figure 4 shows examples of descriptions of the energy pattern of the total cross-section for the $^{3}He(t,d)^{4}He$ reaction for two types of calculation. The spline curve coefficients found are shown in Table 6.

The total cross-section can be found from the formula:

$$\sigma_t(E) = A_0^{(i)} + A_1^{(i)}(E - E_i) + A_2^{(i)}(E - E_i)^2 + A_3^{(i)}(E - E_i)^3,$$

where i is the number of the spline node; $E_i < E < E_{i+1}$.